Title: Fiber pumps for wearable fluidic systems

Authors: Michael Smith[1]*, Vito Cacucciolo[1,2], Herbert Shea[1]*

Affiliations:

[1]Soft Transducers Laboratory (LMTS), École Polytechnique Fédérale de Lausanne; Neuchâtel, Switzerland.

[2]Department of Mechanics, Mathematics and Management (DMMM), Politecnico di Bari; Bari, Italy.

*Corresponding authors. Email: michael.smith@epfl.ch, herbert.shea@epfl.ch

Abstract:

Incorporating pressurized fluidic circuits into textiles can enable muscular support, thermoregulation and haptic feedback in a convenient wearable form-factor. However, conventional rigid pumps, with their associated noise and vibration, are unsuitable for most wearables. We report fluidic pumps in the form of stretchable fibers. This allows pressure sources to be integrated directly into textiles, enabling untethered wearable fluidics. Our pumps consist of continuous helical electrodes embedded within the walls of thin elastomer tubing, and generate pressure silently via charge-injection electrohydrodynamics. Each meter of fiber generates 100 kPa of pressure while flowrates approaching 55 ml/min are possible, equivalent to a power density of 15 W/kg. The benefits in design freedom are considerable, which we illustrate with demonstrations of wearable haptics, mechanically active fabrics and thermoregulatory textiles.

One-Sentence Summary:

Fluidic pumps are fabricated in a fiber format and enable highly integrated, wearable soft robotics.

Main Text:

The widespread use of textiles, and their close contact with the human body, make functional fabrics an attractive technology for wearable devices. When creating technology that is meant to be worn, fiber-format components offer several advantages due to their flexibility, scalability and compatibility with existing textile production techniques (*1*, *2*). Fiber-based actuators (*3*), sensors (*4*), energy storage (*5*) and energy harvesting (*6*) devices demonstrate the progress in this field and the benefits afforded by this format.

Notably lacking, however, are fiber-based fluidic components. Fluidic actuation is fundamental to much of soft robotics, a key axis of wearable technology (*7*, *8*). Fluidic systems also enable numerous other processes, including heat and mass transport, within conventional medical, industrial and personal devices. The lack of active fluidic components that can be straightforwardly integrated into textiles is inhibiting the development of countless useful devices – devices such as soft supportive exoskeletons, adaptive medical orthoses and wearable haptics.

Generating meaningful fluidic power (the product of pressure and flowrate) in a wearable and portable manner remains a significant challenge. While several 'soft' pumps made entirely from compliant materials have recently been reported (*9–13*), their low levels of power density hinder untethered wearable applications. Furthermore, none of these pumps has a form factor which can be woven into a textile, and none demonstrate the scalability necessary for human-sized applications.

We present a fluidic pump in the form of a fiber (Fig. 1A). The pump is a flexible and stretchable tube, of order millimeters in diameter, which can generate continuous fluid flow without any moving parts or vibration. The amount of pressure and flowrate generated by the fibers is a function of both their length (Fig. 1E) and diameter (Fig. 2B).

The fiber pumps are able to pump liquid in a form factor which is inherently compatible with wearable devices (Fig. 1F). In generating flow directly within the tubing itself (Fig. 1G), the need for an external pump is removed and fluidic systems can be significantly simplified. This affords substantial improvements in design freedom for wearables. Pumps can be distributed throughout the volume of the device, reducing losses, improving comfort and enabling advanced multi-pump wearables without the need for valves and connectors. The distributed nature of the fiber pumps means that the weight of the pump can be counted against the weight of tubing required in a

conventional fluidic circuit. In the case of fiber pumps, the tubing is the pump, and effectively the pump comes at no extra weight penalty.

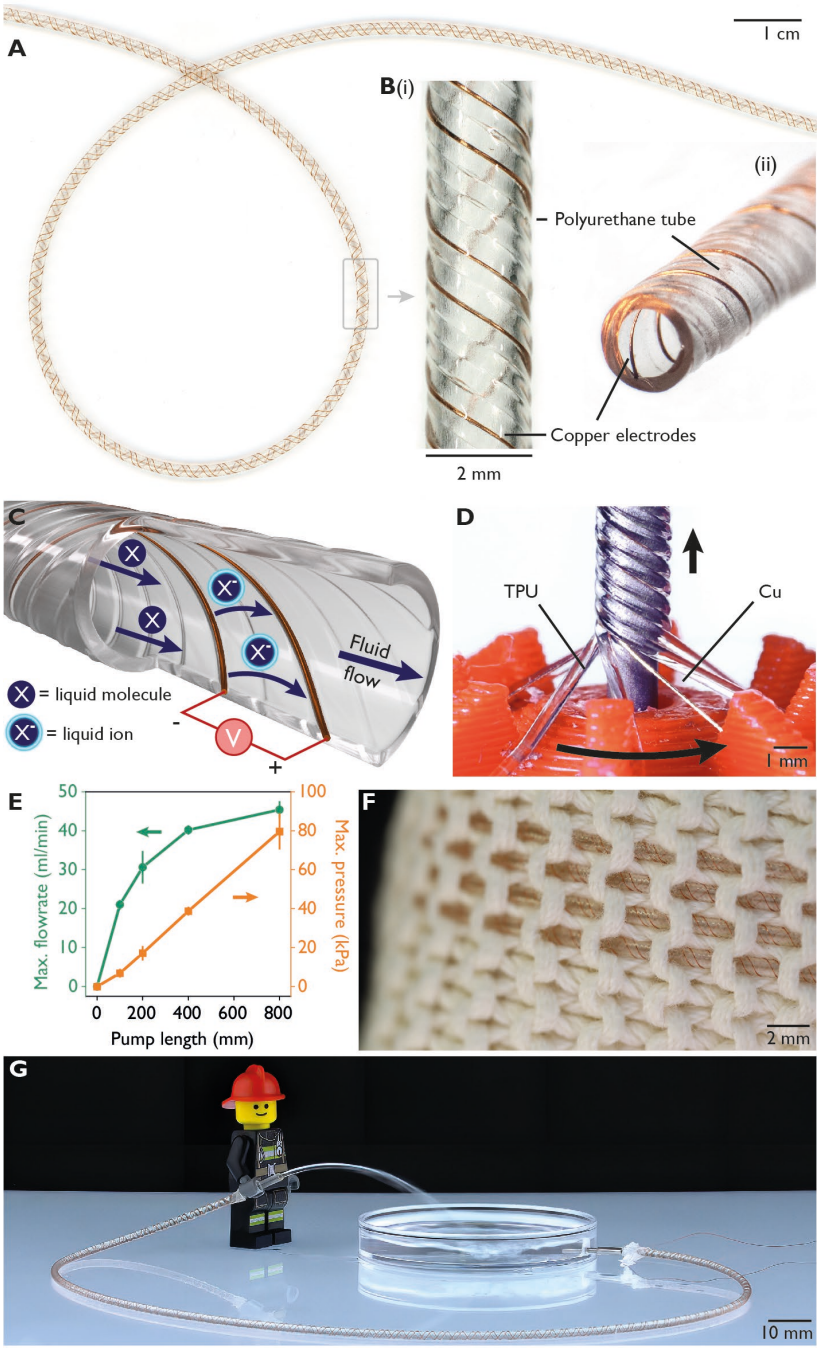

Fig. 1. A fiber-format electrohydrodynamic pump. (**A**) The fiber pump is soft and flexible. (**B**) The structure of the fiber pump (i), showing the helical copper electrodes embedded within the walls of a polyurethane tube (ii). (**C**) A schematic illustration of the pump operating principle. Liquid molecules become ionized at the negative electrode, accepting an electron. The ions are then accelerated to and discharged at the positive electrode, generating a net fluid flow. (**D**) Pumps are fabricated using a filament winding method. (**E**) The scaling of fiber pump pressure and flow

rate with pump length, for an 8 kV/mm applied electric field. Values are mean ± SD for $N = 3$ pumps of each length. **(F)** The fiber pumps sewn into a woolen textile. (**G**) The fiber pump in operation. See also Movie S1.

Fiber pump fabrication and performance

The pumps operate using the principle of charge injection electrohydrodynamics (EHD) (*9*, *14–16*). Embedded in the pumps' polyurethane tube wall are two continuous helical electrodes, fabricated from copper wire (80 μm diameter). Applying a d.c. electric field up to 8 kV/mm between these electrodes ionizes a dielectric liquid within the tube, creating negatively charged ions as liquid molecules accept electrons. These ions are accelerated towards the positive electrode, where they discharge. As they move, they set in motion the surrounding liquid molecules to create a net fluid flow (Fig. 1C). The asymmetrical spacing of the helical electrodes ensures that, for a given polarity of applied voltage, there is a net flow in one direction. Inverting the polarity of the applied voltage will reverse the direction of flow (see Fig. S7A).

Helical configurations of electrodes have previously been simulated for use in EHD conduction pumps (a related but distinct pumping mechanism) (*17*). We demonstrate that this configuration can produce exceptional performance as an ion-drag EHD pump. Pressures exceeding 80 kPa and flowrates approaching 55 ml/min are reported here. Considering the weight of the pump, this corresponds to power densities in excess of 15 W/kg, substantially larger than previous attempts at soft pumps and within a factor of two of class-leading (rigid) miniature pumps (see Table S3). Furthermore, this configuration is up to ten times more efficient than a conventional layout of interdigitated electrodes (*9*), can generate 30 times the pressure response rate (Fig. 2F) and results in a stable, repeatable device (Fig. S6).

The structure of the fiber pumps is created using a filament winding fabrication method (Fig. 1D, Fig. S5 and Movie S2). This involves simultaneously twisting thermoplastic polyurethane (TPU) filament and copper wire together around a central mandrel and subsequently fusing the filament together with heat. Removing the mandrel reveals a hollow tube with helical electrodes embedded within the walls (*18*). Crucially, these electrodes remain exposed along the inner surface of the tube wall (Fig. 1B(ii)), enabling the injection and collection of charge necessary for EHD pumping. The filament winding method is continuous and allows for a simple pump construction from only two materials. This greatly reduces the compatibility issues between pump materials and EHD liquids that were previously reported (*9*).

This same fabrication method can be used to create different pump geometries. The exact structure is determined by the close packing of the TPU filaments around the mandrel, which is dependent on the number of filaments, their diameter and the diameter of the mandrel (see supplementary text and Fig. S1). Changing the mandrel diameter leads to different diameter pumps (Fig. 2A). Since the structure is helical, however, pump diameter cannot be changed independently – some other aspect of the structure must also change. For the pumps in Figure 2, the helix angle has been kept constant at approximately 60 ° by changing the number of filaments for each diameter (see Table S1). Consequently, the helix pitch is different in each case.

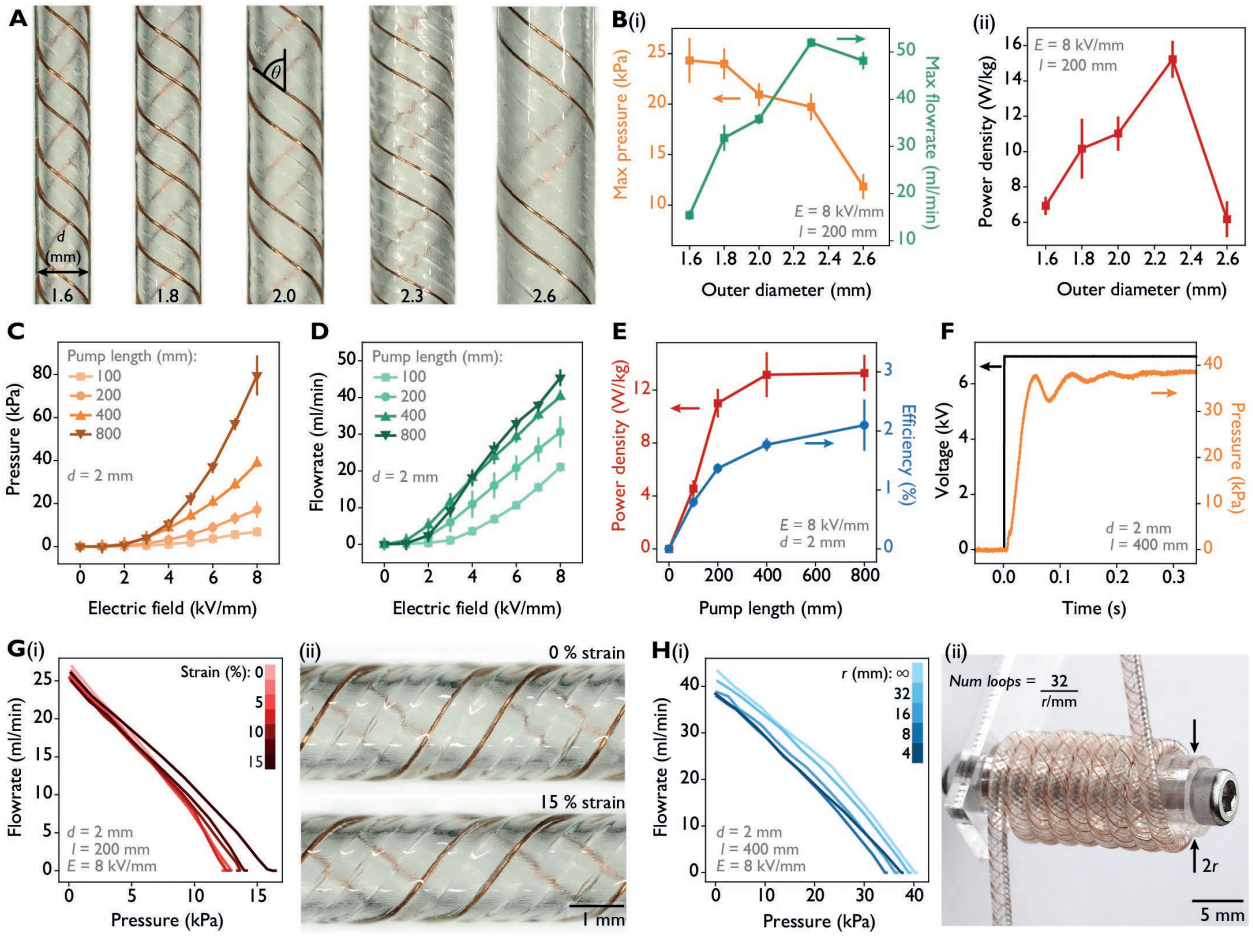

Fig. 2. Characterisation of the fiber pumps. Values with error bars correspond to mean ± SD for $N = 3$ pumps. (**A**) Fiber pumps fabricated at different diameters with an approximately constant helix angle $\theta \sim 60$ °. (**B**) Variation in (i) maximum pressure & flowrate and (ii) power density for the different pump diameters at a constant helix angle of 60 °. (**C**) Pressure and (**D**) flowrate scaling with applied electric field for various pump lengths, all with 2 mm outer diameter. (**E**) The power density and efficiency as a function of pump length, for a 2 mm diameter pump at 8 kV/mm. (**F**) Pressure and voltage as a function of time. Maximum stable pressure is reached within 200 ms. The oscillations in the pressure measurement are due to the elasticity of the pump and connecting

tubing. (**G**) (i) The pressure-flowrate characteristics of a fiber pump at different levels (ii) of uniaxial strain. (**H**) (i)The pressure-flowrate characteristics of a fiber pump subjected to different radii of curvature (*r*). Curvature is achieved by wrapping the pump around circular objects with multiple loops (ii) to ensure an equal length of pump was deformed in each case

Under these conditions, reducing the pump diameter increases the maximum pressure but decreases the maximum flowrate (Fig. 2B(i)). A maximum power density of 15.2 W/kg occurs at a diameter of 2.3 mm (1.5 mm inner diameter) (Fig. 2B(ii)), although the optimum helix angle and pitch are likely different for each diameter (see supplementary text and Fig. S2). The electrode spacing can be controlled independently of diameter, and is set by the number of TPU filaments between the copper wires. In all cases here, two filaments are used, giving a (perpendicular) electrode spacing of 800 μm. We anticipate that the pump structure can be optimized further, leading to additional improvements in performance.

With respect to the applied electric field, the maximum pressure scales non-linearly (Fig. 2C), as is typically seen in charge-injection EHD pumps (*15*). Maximum flowrate scales linearly with applied field once above a value of 5 ml/min (Fig. 2D), a behavior also seen in other EHD pumps (*15*, *19*). Peak power density and efficiency both increase with increasing pump length (Fig. 2E) and electric field (Figs. S7E & S7F). The fiber pumps can pump continuously for up to 6 days before chemical deposits passivate the electrodes (Fig. S7H). This is considerably longer than any other reported EHD pump, soft or otherwise (*9*), and can likely be improved further through careful selection of liquid and electrode material.

Throughout this work we used the dielectric liquid Novec 7100 (3M). This is a non-toxic, non-flammable methoxy-fluorocarbon with low global warming potential (*20*). It is commonly used as a solvent and for heat management, but also performs well as an EHD fluid due to readily ionizable fluorine groups and a high electrical breakdown field of 10 kV/mm (*20*). Other liquids (including non-fluorinated compounds) may be pumped, provided they have low conductivity, low viscosity and are electrochemically stable (*21*, *22*).

The electric fields used to drive these pumps equate to voltages on the order of kilovolts. This is necessary to overcome the energy barrier for ionization of the liquid. However, the amount of current flowing is low (< 110 μA, Fig. S7I). This results in a low power consumption of approximately 0.9 W/m. Consequently, the fiber pumps can be powered with a battery-operated

high voltage power supply, weighing 35 g (including battery, see Fig. S11), enabling untethered operation (Movie S1). A typical smartphone battery would power a 1 m length of pump continuously for approximately 15 hours.

Pump flexibility and stretchability

A major attraction of fiber-based technologies is the compliance offered by this format. The fiber pumps are flexible about every direction perpendicular to their axis, offering significant design freedom for integration into wearables and highly compliant soft actuators. It is important, therefore, to understand how the fiber pumps behave when deformed. Stretchability is assessed by measuring the pressure-flowrate characteristics of the pump – known as the 'pump curve' – at different values of uniaxial strain (Fig. 2G). Even at 15 % strain (a strain level sufficient for wearable applications), pump performance is broadly unchanged. Beyond 25 % strain, the pump will begin to fail as the electrode structure detaches from the tube wall (Fig. S8). It is also worth noting that this stretchability is achieved using conventional materials: the helical nature of the electrodes means that a stretchable device can be fabricated without lossy and unreliable stretchable conductive materials (Fig. 2G(ii)).

Figure 2H(i) displays the pump curves captured as the fibers are deformed to different radii of curvature. To enable a fair comparison between different curvatures, the number of loops is adjusted to ensure that an equal length of pump is deformed in each case (Fig. 2H(ii)). Deforming to a bend radius of 4 mm – four times the radius of the pump itself – reduces the maximum pressure by 7 % and maximum flowrate by 12 % when compared to an undeformed pump. The slight reduction can be explained by considering the change in electrode spacing around the inside and outside of the deformed pump, as well as the pressure loss inherent to fluid flow through a curved tube. The pump will kink if subjected to a sufficiently low bend radius, typically < 3 mm, although the exact value will depend on the loading conditions and pump dimensions (*23*). The kink, however, does not damage the pump structure and the pump can continue to operate once the kink is removed (Fig. S8 and Movie S9).

Under repeated uniaxial strain, the pumps can withstand at least 5000 cycles to 10 % strain without change in performance (Fig. S9). Repeated flexion to a bend radius of 3 mm for 5000 cycles has no effect on pump performance (Fig. S10).

Fiber and textile-based actuators with fiber pumps

The ability of these pumps to generate substantial flowrates and pressures while maintaining flexibility permits multiple applications in textile-based and wearable applications, which previously required an external conventional pump. We demonstrate the fiber pumps in the context of mechanically active fibers and textiles (Fig. 3), as well as thermoregulatory wearables for heat management and haptic feedback (Fig. 4).

Actuation can be achieved using fiber-like artificial muscles, similar in concept to inverse pneumatic artificial muscles (IPAMs) (*24*), but operating with a liquid rather than a gas. These inverse hydraulic artificial muscles (IHAMs) can be integrated directly with the fiber pumps (Fig. 3A & Movie S8). The IHAM consists of an elastic tube with a helix of inelastic thread embedded within its walls. This thread acts as a radial constraint such that, as the IHAM is pressurized by the fiber pump, the device does not expand radially but instead extends along its length (Fig. 3B). Actuation is fast (Fig. 3C) due to the low internal volume of the actuator (~ 300 µl) and the high performance of the fiber pump. A single fiber exerts a maximum difference in isometric axial force of ~ 0.5 N, and actuators can be used in parallel to increase force output (Fig. 3D). Response to the applied voltage is repeatable, with low hysteresis (Fig. 3E). The fast time response of the fiber IHAMs facilitates operation beyond the quasi-static regime (Fig. 3F), where they can continue to operate for several thousands of cycles (Fig. 3G).

Figure 3H demonstrates how the fiber pumps can be integrated directly into textiles to create active fabrics. The device shown consists of a fluidic fabric muscle (*25*) with a fiber pump woven directly into the fabric (Fig. 3I). The operating principle is similar to that of the IHAMs, except here the radial constraint is supplied by an inextensible fabric sewn around the elastic tubing. The result is an active fabric, capable of changing shape upon electrical command (see Movie S7). Operating at an applied field of 8 kV/mm, maximum strains approaching 40 % are possible (see Fig. S12D) while actuation strains of 16 % are reached with an applied load of 100 g (Fig. 3H). A maximum isometric axial force of 1.7 N is achieved, controllable by tuning the pump voltage (Fig. 3J). Actuation speed is reduced due to the larger internal volume, yet nonetheless full actuation occurs in under 20 s, an adequate timeframe for wearable applications such as self-adjusting clothing and intermittent compression devices. The entire device can also be washed using standard laundry detergent (Fig. S13 and Movie S10) without compromising its performance.

The example actuators shown here utilize the pump working fluid directly. It is equally feasible to instead use this fluid to displace a second fluid, such as air, to allow existing pneumatic actuators to be used without modification.

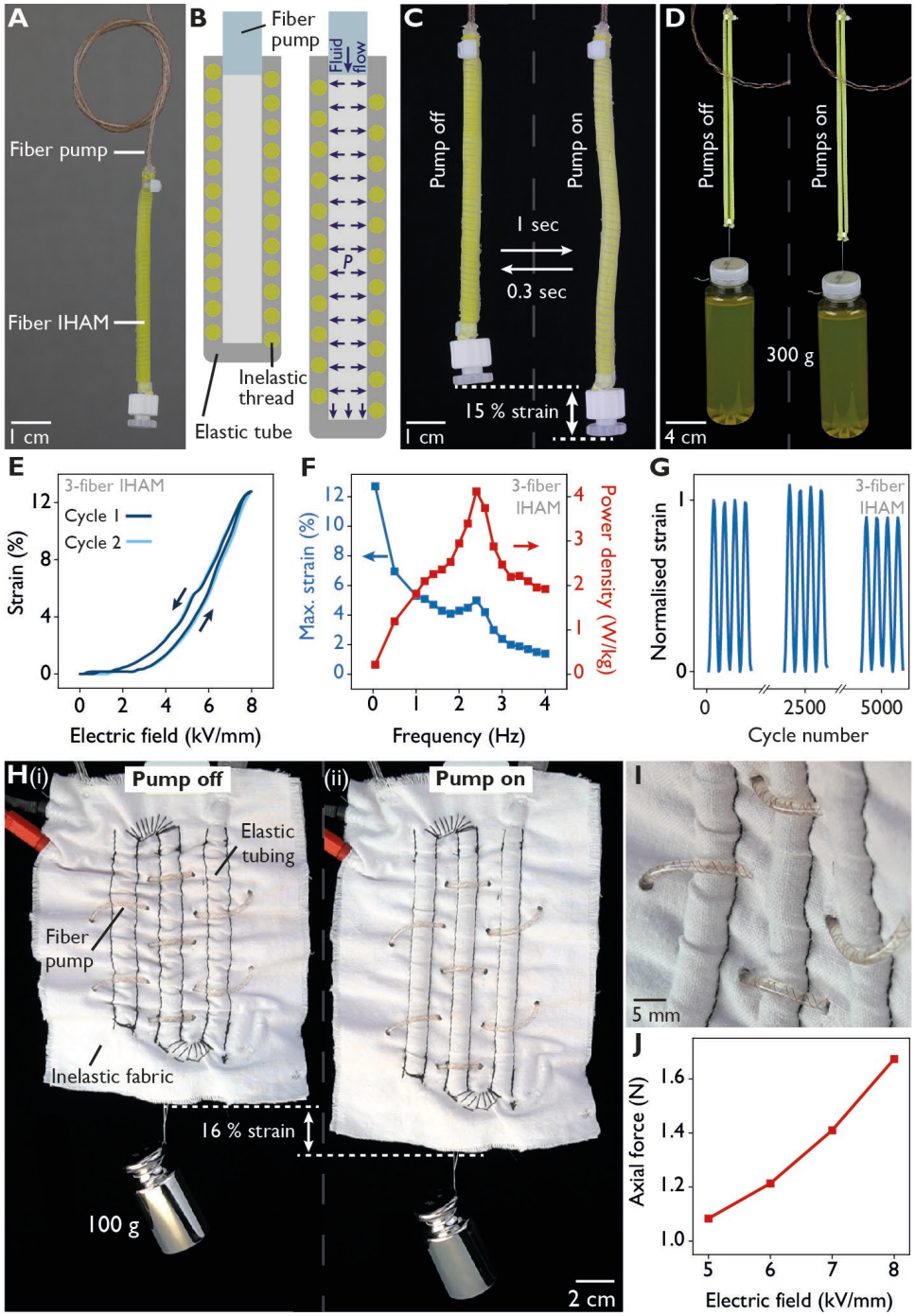

Fig. 3. Actuators powered using fiber pumps. (**A**) A fiber pump connected to a 9 cm long inverse hydraulic artificial muscle (IHAM). (**B**) The IHAM consists of helices of inelastic thread embedded within the wall of an elastic tube. (**C**) A maximum strain of 15% is achieved from a single fiber. (**D**) Combining IHAMs and pumps in parallel can generate higher forces. Here, three

IHAMs and pumps are used to move a 300 g load. (**E**) The strain of the 3 fiber IHAM as a function of the electric field applied to the fiber pumps. (**F**) The frequency response of the 3-fiber IHAM moving a 200 g weight. Applied signal is 6.4 kV square wave (equivalent to 8 kV/mm). A small resonance peak is observed at ~ 2.4 Hz (**G**) The 3 fiber IHAM can operate for at least 5000 cycles at 2.4 Hz with minimal loss in amplitude. (**H**) A fluidic fabric actuator with integrated fiber pump. In this device, an elastic tube is sewn between two sheets of inextensible fabric. The ruffling of the fabric allows the actuator to extend when pressurized. (**I**) The fiber pump integrated directly into the fabric actuator. (**J**) The maximum difference in isometric axial force generated by the actuator as a function of the applied electric field.

Thermoregulation and thermal haptics using fiber pumps

We also demonstrate two applications of fiber pumps in thermally active textiles. Figure 4A shows a thermal haptic glove, a class of device used to generate different temperature sensations to enhance the sense of immersion in virtual reality (*26*). Typically reliant upon rigid thermoelectric ceramics, here we demonstrate how a thermal haptic glove can be realized using soft and flexible fiber pumps.

The glove consists of a reservoir of chilled Novec 7100 fluid and five separate, independently controlled fiber pumps winding around the fingers. Activating a pump rapidly flows cold fluid around the finger (Fig. 4B), chilling the pump to the fluid temperature within 2 seconds and providing a thermal haptic stimulus to the user (Movie S4). Once the pump voltage is removed and without the constant flow of chilled fluid from the reservoir, the pump returns to room temperature. In a virtual reality setting, this allows the temperature and thermal properties of objects to be simulated with a degree of spatiotemporal resolution: the physical object that represents the virtual one can be made to feel cold, and that sensation is felt only through those fingers in contact with the object (Fig. 4C). Achieving the same effect with any other pump would require several separate pumps or an array of valves, hindering wearability.

The same principle can be applied to an entire garment (Fig. 4D). Four sections of fiber pump transport chilled fluid around the torso and arms. The pumps are powered with a battery-operated power supply (Fig. S11), creating an untethered system that can be used in any environment and during physical activity (see Movie S5). As well as enabling untethered operation, the low power consumption of the pumps means that Joule heating is negligible in comparison to the cooling rate provided by the chilled fluid.

The concept of thermoregulatory fabric can be developed further, as shown in Figure S14. The pump fibers themselves can be woven together to create a fluidic fabric, which when attached to hot and cold reservoirs of fluid, allows the temperature of the fabric to be regulated (Movie S6). Such a patch of woven pumps can also be considered as a pressure source, sewn directly into the textile of a wearable device to provide high pressure fluid for actuation.

Concluding remarks

We have demonstrated a fluidic pump in the form of a flexible fiber which is capable of generating exceptional pressures and flowrates. This advancement allows rigid and bulky external pumps to be removed from wearable fluidic devices – effectively turning the tubing into the pump. The scalability, simplicity and stability of both the operation and fabrication of these fibers enables applications that are not possible with conventional pumping technologies.

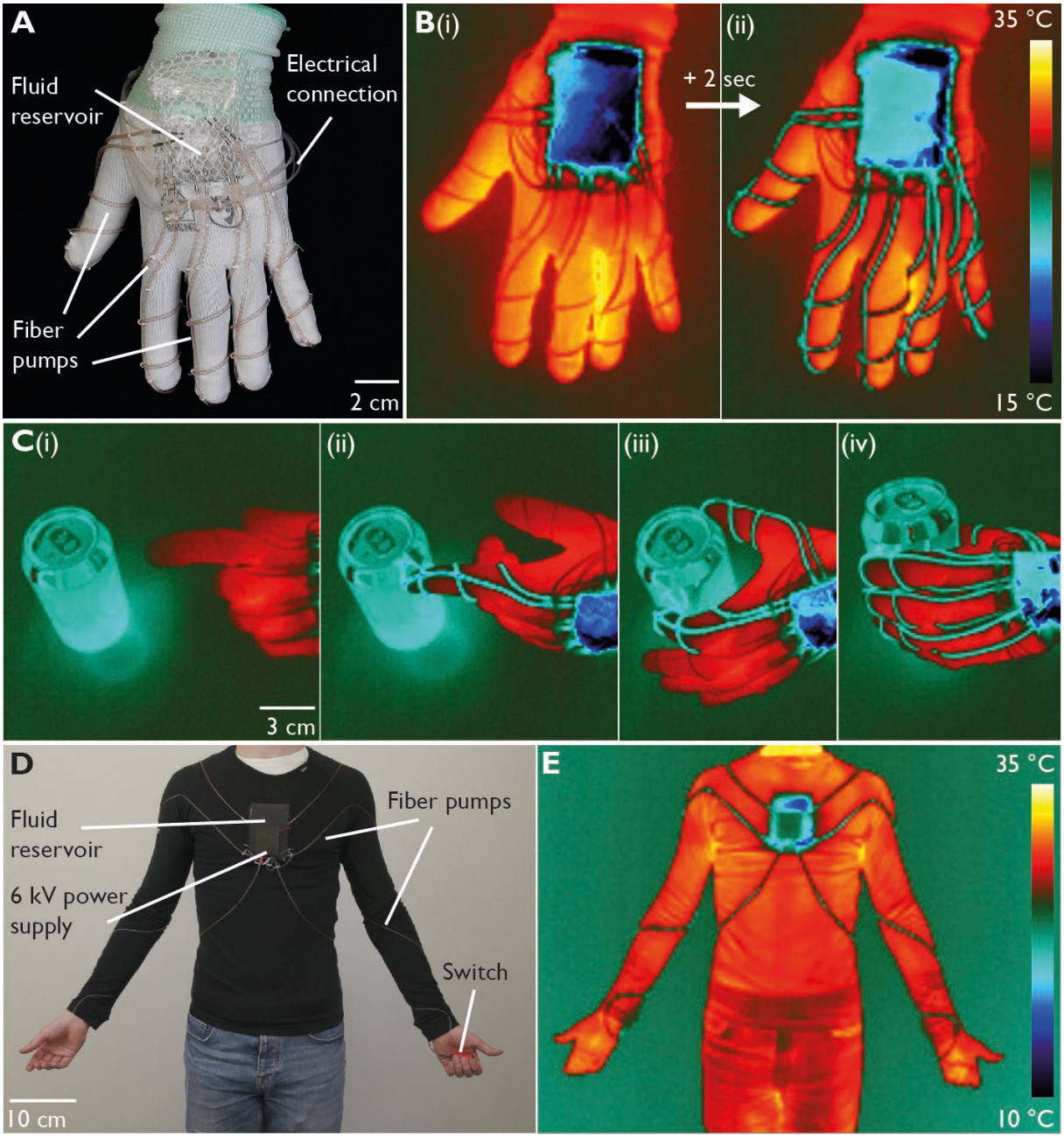

Fig. 4. Heat management using fiber pumps. (**A**) A thermal haptic glove with separate, individually controlled fiber pumps attached to each finger. (**B**) Thermal images of the glove (i) before and (ii) 2 seconds after simultaneously activating all pumps. (**C**) A demonstration of thermal haptic feedback: (i) approaching the object with no pumps active, (ii) activating the pump of the finger in contact with the object, chilling the finger and providing a thermal haptic stimulus, subsequently activating the thumb (iii) and remaining fingers (iv) as they come into contact with the object. (**D**) A fully wearable and untethered thermoregulatory garment, with integrated fiber pumps, power supply and fluid reservoir.

References and Notes

1. G. Loke, W. Yan, T. Khudiyev, G. Noel, Y. Fink, Recent Progress and Perspectives of Thermally Drawn Multimaterial Fiber Electronics. *Advanced Materials*. **32**, 1904911 (2020).

2. J. Xiong, J. Chen, P. S. Lee, Functional Fibers and Fabrics for Soft Robotics, Wearables, and Human–Robot Interface. *Advanced Materials*. **33**, 2002640 (2021).

3. C. S. Haines *et al.*, Artificial Muscles from Fishing Line and Sewing Thread. *Science*. **343**, 868–872 (2014).

4. W. Yan *et al.*, Single fibre enables acoustic fabrics via nanometre-scale vibrations. *Nature*. **603**, 616–623 (2022).

5. T. Khudiyev *et al.*, Thermally drawn rechargeable battery fiber enables pervasive power. *Materials Today*. **52**, 80–89 (2022).

6. H. Sun, Y. Zhang, J. Zhang, X. Sun, H. Peng, Energy harvesting and storage in 1D devices. *Nat Rev Mater*. **2**, 1–12 (2017).

7. T. Abe, S. Koizumi, H. Nabae, G. Endo, K. Suzumori, "Muscle textile to implement soft suit to shift balancing posture of the body" in *2018 IEEE International Conference on Soft Robotics (RoboSoft)* (2018), pp. 572–578.

8. O. Kilic Afsar *et al.*, "OmniFiber: Integrated Fluidic Fiber Actuators for Weaving Movement based Interactions into the 'Fabric of Everyday Life'" in *The 34th Annual ACM Symposium on User Interface Software and Technology* (Association for Computing Machinery, New York, NY, USA, 2021; https://doi.org/10.1145/3472749.3474802), *UIST '21*, pp. 1010–1026.

9. V. Cacucciolo *et al.*, Stretchable pumps for soft machines. *Nature*. **572**, 516–519 (2019).

10. Y. Matia, H. S. An, R. F. Shepherd, N. Lazarus, Magnetohydrodynamic levitation for high-performance flexible pumps. *Proc. Natl. Acad. Sci. U.S.A.* **119**, e2203116119 (2022).

11. R. S. Diteesawat, T. Helps, M. Taghavi, J. Rossiter, Electro-pneumatic pumps for soft robotics. *Science Robotics*. **6**, eabc3721 (2021).

12. W. Tang *et al.*, Customizing a self-healing soft pump for robot. *Nature Communications*. **12**, 2247 (2021).

13. C. Stergiopulos *et al.*, "A Soft Combustion-Driven Pump for Soft Robots" in *ASME 2014 Conference on Smart Materials, Adaptive Structures and Intelligent Systems* (American Society of Mechanical Engineers Digital Collection, 2014; https://asmedigitalcollection.asme.org/SMASIS/proceedings/SMASIS2014/46155/V002T04A011/286215).

14. A. Ramos, Ed., *Electrokinetics and Electrohydrodynamics in Microsystems* (Springer Vienna, Vienna, 2011; http://link.springer.com/10.1007/978-3-7091-0900-7).

15. J. Kim, Y. Yamada, S. Yokota, Micro ECF (electro-conjugate fluid) hydraulic power sources based on the modular design of TPSEs (triangular prism and slit electrode pairs). *Int J Adv Manuf Technol*. **106**, 627–639 (2020).

16. Z. Mao, T. Iizuka, S. Maeda, Bidirectional electrohydrodynamic pump with high symmetrical performance and its application to a tube actuator. *Sensors and Actuators A: Physical*. **332**, 113168 (2021).

17. N. O'Connor, J. Yagoobi, "An Innovative EHD Conduction Pumping Design for Swirl Flow Generation" in *2021 IEEE Industry Applications Society Annual Meeting (IAS)* (2021; https://ieeexplore.ieee.org/document/9677332), pp. 1–6.

18. See Materials and Methods section of the supplementary materials for a detailed account of pump fabrication. See also Figure S5 and Movie S2.

19. T. Matsubara, H. H. Huynh, K. Yoshida, J. Kim, Development of MEMS-fabricated bidirectional ECF (electro-conjugate fluid) micropumps. *Sensors and Actuators A: Physical*. **295**, 317–323 (2019).

20. M. S. EL-Genk, H. Bostanci, Saturation boiling of HFE-7100 from a copper surface, simulating a microelectronic chip. *International Journal of Heat and Mass Transfer*. **46**, 1841–1854 (2003).

21. S. Yokota, Y. Otsubo, K. Edamura, Electro-sensitive movable fluids, methods of using the same and motors for the electro-sensitive movable fluids (2000), (available at https://patents.google.com/patent/US6030544A/en).

22. J. E. Bryan, J. Seyed-Yagoobi, Experimental Study of Ion-drag Pumping Using Various Working Fluids. *IEEE Transactions on Electrical Insulation*. **26**, 647–655 (1991).

23. K. Luo, P. Rothemund, G. M. Whitesides, Z. Suo, Soft kink valves. *Journal of the Mechanics and Physics of Solids*. **131**, 230–239 (2019).

24. E. W. Hawkes, D. L. Christensen, A. M. Okamura, "Design and implementation of a 300% strain soft artificial muscle" in *2016 IEEE International Conference on Robotics and Automation (ICRA)* (2016), pp. 4022–4029.

25. M. Zhu, T. N. Do, E. Hawkes, Y. Visell, Fluidic Fabric Muscle Sheets for Wearable and Soft Robotics. *Soft Robotics*. **7**, 179–197 (2020).

26. Y. Huang *et al.*, Recent advances in multi-mode haptic feedback technologies towards wearable interfaces. *Materials Today Physics*. **22**, 100602 (2022).

Acknowledgments:

The authors thank V. Py and M. Benbedda for assistance with the high voltage electronics featured in this work. We thank S. Maeda and F. Hartmann for helpful discussions. We also thank J. La Scala for developing the automated fabrication system used in this work. Thanks also to L. Caillaud and E. Valicka for help in creating the textile-based demonstrations. Further thanks to E. Valicka and R. Hennig for assistance with videography and video editing.

Funding: We acknowledge the support of the Swiss National Science Foundation (grant no. IZLJZ2_183656)

Author contributions: M.S., V.C. and H.S. formulated the concept; M.S. fabricated the devices, carried out the experiments, analyzed the data and created the figures & videos with supervision from H.S. and V.C; M.S. prepared the original draft of the manuscript; M.S., V.C. and H.S. reviewed and edited the manuscript.

Competing interests: The authors declare no competing interests.

Data and materials availability: All data that support the claims in this manuscript are available on the Zenodo repository (DOI: 10.5281/zenodo.7451722).

Supplementary Materials

Materials and Methods

Supplementary Text

Figs. S1 to S14

Tables S1 to S3

Movies S1 to S10

Science
AAAS

Supplementary Materials for

Fiber pumps for wearable fluidic systems

Michael Smith, Vito Cacucciolo, Herbert Shea

Correspondence to: michael.smith@epfl.ch, herbert.shea@epfl.ch

This PDF file includes:

Other Supplementary Materials for this manuscript include the following:

Materials and Methods

Pump fabrication

The fiber electrohydrodynamic (EHD) pumps are fabricated via a filament winding method (Fig. S5 and Movie S2). Thermoplastic polyurethane (TPU) threads and copper (Cu) wire are twisted together around a central mandrel. This process simultaneously creates the pump body and the double-helix electrodes.

Prior to winding, TPU thread is prepared by extruding 3D printer filament (Recreus Filaflex 70A) through a circular 0.4 mm nozzle at 230 °C. Cu wire of 80 μm diameter (Block, 50/0.08) is prepared by mechanically removing the enamel coating using a razor blade. Weights of approximately 60 g and 20 g are attached to the TPU thread and Cu wire, respectively, before being loaded into the winding apparatus.

The winding apparatus consists of a rotary stage coupled with a linear actuator. The respective angular and linear velocities of the stages are programmatically controlled to ensure the correct winding angle. A 3D printed guide attached to the rotary stage ensures the filaments and wire follow a repeatable path to the mandrel. As the filaments are wound together, the copper wire fits underneath the polyurethane threads, resting directly against the central mandrel. As winding continues, the copper wire is effectively held in place by the TPU threads, securing the structure and preventing the helical electrodes from being disturbed during the manufacturing process

The values of the weights attached to the filaments are important to ensure a controlled and repeatable winding process. The tension in the TPU thread must be sufficient to keep them taught and held firmly against the mandrel while winding. For the Cu wire, the tension must be large enough to ensure the wire gets pulled between the TPU threads while winding, but not so large as to cause the structure to slip or break the wire.

Towards the end of the winding, Cu wire is cut and lifted through the guide, such that the end of the winding process continues for ~ 15 mm with only TPU thread. At the other end, the copper wire is cut and manually unwound for ~ 15 mm. This ensures that the ends of the pump are free of Cu wire electrodes, allowing straightforward fluidic connection.

Once wound, the structure is clamped at either end using cable ties and removed from the winding apparatus. A small amount of cyanoacrylate glue (Loctite 431) is applied where the copper wire exits the structure. Once set, the mandrel is placed in a pre-heated oven at 180 °C for 18 minutes. This heat treatment is sufficient to melt and fuse the TPU threads to create a sealed tube.

Prior to winding, the mandrel is coated with mold release spray (Mann Release Technologies, Ease Release 200), such that the pump can be easily removed once fused. The pump is flushed with isopropyl alcohol after removal to remove any residual release spray.

The winding set up allows for fibers up to 400 mm to be fabricated in one piece. For longer lengths of pump, sections of fiber can be connected by fusing the ends together with heat, soldering the electrode wires together and covering the junction with heat-shrink tubing or silicone epoxy (Sil-poxy, Smooth-on).

Different pump diameters are created by using different diameter mandrels (Modelcraft spring steel wire, P/N 294764, conrad.com). Table S1 describes the conditions used to fabricate pumps of different diameter but with an approximately equal helix angle of ~ 60°. For a 0.8 mm mandrel, creating a higher helix angle to better match the others would require 4 filaments. However, keeping the same two-filament electrode spacing, this would give a symmetrical electrode structure. We have therefore used 5 filaments, despite the helix angle not being the same. All of the pumps used for the diameter scaling investigation are 200 mm long.

Pump performance characterisation

For all characterisation experiments and demonstrations, Novec 7100 (3M) is used as the dielectric fluid. Fresh fluid is used for each pump tested. The pumps are characterized using a specially designed fluidic circuit (Fig. S4). This consists of the pump itself, a flowrate sensor (Fluigent FLU-XL), a pressure sensor (Copal Electronics PA-750-352G-R2), a fluid reservoir and a motorised pinch valve (Resolution Air MPPV-4). High purity tubing (Versilon C-210-A) is used to connect the elements of the circuit to minimize interaction with the dielectric fluid.

This circuit allows the pressure-flowrate behavior of the pump – the 'pump curve' - to be captured. Initially, the pump is turned on as the pinch valve is completely open, such that the maximum flowrate is observed. The pinch valve is then incrementally closed, increasing the fluidic impedance of the circuit, thereby reducing the flowrate and increasing the pressure. The pressure and flowrate data acquired at each valve-closure set-point becomes a single data-point on the pump curve. Eventually, the valve is completely closed and the maximum pressure condition is reached. The procedure can then be repeated for a different applied voltage. This measurement sequence is automated using Python code, which handles the valve-position, applied voltage and data collection.

All measurements are conducted using a high voltage power supply consisting of an Arduino Micro microcontroller and an EMCO CB101 10 kV DC/DC converter. One exception to this is the response time measurement (Fig. 2, main text), where a Trek 10/10B-HS high voltage amplifier is used to achieve the required voltage slew rate. A 10 MΩ resistor is placed in series with the pumps to limit current in case of a breakdown. The voltage drop across this resistor is calculated and accounted for in the pump data analysis.

For voltage, diameter and length scaling experiments, data points represent the mean value taken from three separate pumps. Error bars represent the standard deviation in the mean. Pump length is defined as the total pump length, including the electrode-free ends.

Pump flexibility and stretchability characterisation

Static strain tests are performed using the characterisation set up shown in Figure S4. Pumps 200 mm in length and with an internal diameter of 1.2 mm are used. One of the fluidic connectors for the pump is able to slide vertically on rails, allowing the pumps to be strained during testing. For the dynamic strain response, the pump is fitted to an Instron tensile test machine (Fig. S9A) to allow cyclic loading. The applied voltage is kept constant during all strain tests.

Static flexibility tests are carried out by wrapping a 400 mm long, 1.2 mm internal diameter pump around laser-cut objects of known diameter. Multiple loops are used to ensure an equal length of pump was deformed in each case. The dynamic flexion response is obtained by fitting a pump (200 mm long, 1.2 mm internal diameter) to a 3D printed scissor mechanism (Fig. S10A). This mechanism is actuated by an Instron tensile test machine to repeatedly flex the pump. The minimum bend radius possible with this mechanism is approximately 3 mm. In both static and dynamic tests, pressure and flowrate values are captured using the characterisation set up shown in Figure S4.

Thermal haptic glove demonstration

For the thermal haptic glove, five separate fiber pumps (1.2 mm internal diameter, 400 mm long) are sewn onto the fingers of a polyamide textile glove. The inlet and outlet of each pump are connected to a common fluid reservoir, mounted to the back of the hand. The fluid reservoir is fabricated from a high-density polyethylene (HDPE) bag fitted with short metal fluid connectors and sealed with hot glue. Water ice packs, also from HDPE bags, are inserted behind the fluid reservoir to chill the dielectric fluid. Both reservoir and ice pack are held in place by a mesh fabric

sewn onto the glove. Electrical connections are established using a high voltage flat-flex cable (McMaster-Carr, part number 9634T206) mounted to the wrist of the glove. A high-voltage switchboard of custom design is used to activate individual pumps. In all images and videos, the pumps are operating at 8 kV/mm (6.4 kV). An infra-red camera (FLIR A15) is used to capture the thermal images.

In this example we have used chilled fluid to demonstrate the concept. This is because while it is relatively simple to fabricate a flexible heating device, achieving cooling in a flexible manner is less straightforward. The same principle can, of course, be used to generate a heating effect.

Thermoregulatory t-shirt demonstration

The thermoregulatory t-shirt consists of four 1.2 m long pump sections (1.2 mm internal diameter) sewn along the arms and torso of a compression base-layer garment. For the pumps attached to the arms, the fluid returns through conventional tubing underneath the garment. A reservoir of dielectric fluid, fabricated from a HDPE bag fitted with fluid connections, is attached to the chest using mesh fabric. A water ice pack is slid behind the reservoir to chill the dielectric fluid. All the pump sections share a common electrical connection and are powered with a battery operated 6 kV power supply (Fig. S8), also mounted in the mesh pocket on the chest. The power supply is operated with a handheld switch routed down the arm of the garment. Thermal images are captured using an infra-red camera (FLIR A15).

Woven pumps demonstration

Two separate pumps (1.2 mm internal diameter, 400 mm long), with separate electric and fluidic connections, are woven together and held in place using a 3D printed frame. One pump is connected to a reservoir of cold fluid, chilled using water ice. The other pump is connected to a reservoir heated to 55 °C using a hot plate. The pumps are operated at 8 kV/mm (6.4 kV), powered with a high voltage switchboard of custom design. An infra-red camera (FLIR A15) is used to capture the thermal images.

Fabric actuator demonstration

The fabric actuator consists of an elastic tube sewn between two sheets of inextensible cotton fabric. As the elastic tube is pressurized, the fabric provides a radial constraint which prevents radial expansion, resulting in the tubing changing in length only. The fabric is purposefully wrinkled perpendicular to the tubing to accommodate this change in length.

The elastic tube is cast from silicone (Ecoflex 0030, Smooth-on) using a 3D printed mold and a 2 mm rod as an inner mandrel. The external diameter is 5 mm. The channels for the bladder are sewn using a machine, while the curved sections are sewn by hand once the bladder is in place. The bladder is fed through the channels using a metal rod. The wrinkling in the fabric is created by repeatedly pulling on the exposed ends of the tube. The friction between the fabric and tube causes the fabric to bunch up as the tubing contracts, creating the desired ruffling effect.

A Luer-type connector is fitted to one end of the elastic tubing. This acts as a port to fill the actuator with fluid and can then be closed during actuation. A fiber pump (1.2 mm internal diameter, 400 mm long) is woven through the fabric and connects to the opposite end of the elastic tube. A short metal tube is fitted to the inlet of the fiber pump and acts as a connector for the fluid reservoir. Electrical connection is made using 2 mm banana plugs.

Actuator extension is measured optically using motion tracking software Kinovea (kinovea.org). Actuator force is measured using an Instron mechanical tester fitted with a 50 N load cell. The actuator is clamped firmly in the test machine and pre-stretched to approximately 30 % strain. This position is held constant as the pump is then turned on. The elastic tubing extends under the pressure generated by the pump, relaxing the pre-strain and therefore reducing the axial force on the actuator. The pump is then turned off, the elastic tubing contracts and the axial force increases. The results are shown as the difference between these two forces levels. Pressure and flowrate are measured throughout the actuation cycles using the sensors from the characterisation set-up described previously.

The washing test is performed by sealing the fluidic channels of the device and then immersing it in 30 °C water with a standard laundry detergent. After 20 minutes of stirring at 300 rpm with a magnetic stirrer, the fabric actuator is removed, rinsed several times in water and left to dry in air. Once fully dry the device is re-filled with Novec 7100 fluid and reconnected to the power supply

Fiber-like inverse hydraulic artificial muscle (IHAM) demonstration

The fiber IHAMs are fabricated using a two-step casting process. In the first step, a 0.75 mm wall thickness tube is cast from silicone (Ecoflex 0030, Smooth-on) using a 3D printed mold and a 2 mm rod as an inner mandrel. The tube remains on the mandrel, which is then mounted into the same winding set-up used to fabricate the fiber pumps. Two threads of fishing line (SpiderWire Stealth smooth, 0.29 mm diameter) are then wound around the outside of the silicone tube with a helix angle close to 90°, such that most of the surface area is covered. Once wound, the mandrel is placed in a second 3D printed mold so that more silicone (Ecoflex 0030, Smooth-on) can be cast around the structure. The second casting adds a further 0.75 mm to the wall thickness, resulting in an overall diameter of 5 mm. The IHAM can then be removed from the mandrel.

Fiber pumps (1.2 mm internal diameter, 400 mm long) are inserted into one end of the IHAM and clamped in place with a cable tie and further sealed with silicone (Sil-poxy, Smooth-on). For the single fiber IHAM, the other end is plugged with a barbed Luer fitting held in place with a cable tie. The ends of the actuators in the 3-fiber IHAM are sealed by clamping against a 3D printed piece with a cable tie. This piece also acts as an attachment for an applied load. A single IHAM fiber with fiber EHD pump weighs 3.6 g. The three fiber IHAM weighs 10 g.

Characterisation is performed with a signal generator and a high voltage amplifier (Trek 10/10B-HS). Strains are measured optically using motion tracking software (kinovea.org). Forces are recorded using an Instron tensile test machine with a 50 N load cell. Power density is calculated by considering the work done per cycle as the actuator contracts with a fixed load (200 g) and the period of the oscillation.

Supplementary Text

1. A basic model for filament winding

It is useful to have a model to predict the structure of a fiber pump fabricated using filament winding – a function that can predict the helix angle (θ) based on the number of filaments used (N), their diameter (d_f) and the diameter of the central mandrel (d_i).

We can arrive at such a relationship by considering the close packing of the TPU helices around inner mandrel. It is possible to express the helix pitch by considering that the cross-section of N filaments must fit exactly within one revolution (Fig. S1A). The cross section of the filaments parallel to the fiber axis is an ellipse (Fig. S1B), with height (s):

$$s = \frac{d_f}{\sin\theta} \qquad (1)$$

And therefore, the helix pitch can also be expressed:

$$h = \frac{N d_f}{\sin\theta} \qquad (2)$$

The pitch of the helix (h) can also be expressed in terms of the internal diameter of the tube, the diameter of the fiber and the helix angle by 'unwrapping' the helix (Fig S1C):

$$h = \frac{\pi\left(d_i + d_f\right)}{\tan\theta} \qquad (3)$$

Equating expressions (1) and (3) leads to the expression for helix angle:

$$\frac{N d_f}{\sin\theta} = \frac{\pi\left(d_i + d_f\right)}{\tan\theta} \qquad (4)$$

$$\cos\theta = \frac{N d_f}{\pi(d_i + d_f)} \qquad (5)$$

This function is plotted in Figure S1D as a function of inner diameter for $N = \{3,4,\ldots,10\}$, using $d_f = 400$ μm. This demonstrates that for a given filament and mandrel diameter, the helix angle is quantized by integer values of N. Figure S1E shows the helix angle for the pumps used in this study, agreeing with the model prediction of helix angle.

2. Optimising the helix angle

We can arrive at a first order estimate of the optimal helix angle by considering the forward and backward flow between the helical electrodes.

The estimate requires some assumptions. First, we assume that only the component of electric field parallel to the fiber axis contributes to the performance. Second, we assume that the pressure generated by an ion-drag EHD pump scales quadratically with electric field. Third, we allow for a linear superposition of forward and reverse flows.

For a forward electric field E_1 and a reverse electric field E_2 (Fig. S2A), the pressure generated by one revolution of electrodes is

$$P = k\left(E_1{}^2 - E_2{}^2\right) \qquad (6)$$

where k is a constant. The electric fields can be expressed in terms of the applied voltage V, electrode spacing parallel to the axis (b) and the helix pitch (h)

$$P = kV^2\left(\frac{1}{b^2} - \frac{1}{(h-b)^2}\right) \qquad (7)$$

The parameters b and h can be expressed in terms of the electrode spacing a, the helix angle θ and the average tube diameter ($d_i + d_f$)

$$P = kV^2\left(\frac{1}{\left(\frac{a}{\sin\theta}\right)^2} - \frac{1}{\left(\frac{\pi\left(d_i + d_f\right)}{\tan\theta} - \frac{a}{\sin\theta}\right)^2}\right) \qquad (8)$$

The optimal helix angle is the angle for which equation 8 is maximized, i.e. $\frac{dP}{d\theta} = 0$. It is most straightforward to find this maximum graphically. For an inner diameter of 1.2 mm, a filament diameter of 400 μm and an electrode spacing of 800 μm, the maximum pressure occurs at a helix angle of ~ 63°. Angles lower than this, while minimizing back flow, generate a smaller pressure component along the length of the fiber. Larger angles maximize the axial pressure component, but also decrease the pitch of the helices, generating more backflow. The optimal angle is also a function of the inner diameter, monotonically increasing with increasing diameter.

3. Length scaling of flowrate

The length scaling of flowrate may at first seem counterintuitive – making a pump longer is equivalent to placing pumps in series, which should leave the flowrate unchanged. However, it is possible to explain this scaling behavior using the experimentally observed pump curves. This also leads to some interesting insight about the EHD pumps.

Figure S3A shows the pump curves from four different lengths of fiber pump (2 mm diameter, all acquired at 8 kV/mm). The gradient of each line is inversely related to the pump length – the gradient of the curve for the 800 mm pump is half that of the 400 mm pump, etc. This implies that all of these lines will intersect at the same point (Fig. S3A). From the experimental data, the pressure at which this occurs is negative. This is because some pressure loss is inevitable in the tubes that connect the pump to the pressure sensor. The result is that all pressure measurements (apart from the max. pressure) are slight underestimates. Nonetheless, some useful insight can still be gained.

Let us assume that the pump curves of different length pumps will all intersect at some value of flowrate (Q_o), as shown in Fig. S3C for pumps of length L_0, $2L_0$ and $4L_0$. Given that the amount of pressure generated by the fiber pumps is linearly related to the pump length (L), the pump curves can be described by the equation

$$Q = Q_0\left(1 - \frac{p}{p_f L}\right) \qquad (9)$$

where p_f is the pressure per unit length generated by the fiber pumps.

The pressures and flowrates that we actually measure correspond the intersection of these curves with the 'system-curve'. This curve describes the pressure-flowrate characteristics of the entire measurement circuit, as determined by the fluidic impedance of the constituent components. The measurement circuit can be considered to consist of an ideal pump with an associated fluidic impedance Z_f and a fluidic impedance to represent the remainder of the circuit (Z_s) (Fig. S3B). Assuming Hagen-Poiseuille type flow, the fluidic impedance of the pump will vary linearly with its length as $Z_f = z_f L$, where z_f is the impedance per unit length of the fiber. Again assuming a linear relationship between pressure and flowrate for the entire circuit, the system curve is given by

$$Q = \frac{p}{Z_s + z_f L} \qquad (10)$$

where p is pressure and Q is flowrate. Note that the system curve will be different for each pump length, since the pump forms a significant part of the fluidic circuit due to its distributed nature.

We can find the operating point of the pumps by solving equations (9) and (10) simultaneously. This leads to the general expressions for operating pressure (p_i) and flowrate (Q_i)

$$Q_i = \frac{Q_0 p_f L}{p_f L + Q_0(Z_s + z_f L)} \qquad (11)$$

$$p_i = \frac{Q_0 p_f L(Z_s + z_f L)}{p_f L + Q_0(Z_s + z_f L)} \qquad (12)$$

Equation (11) describes the length dependence of the measured flowrate. Fig. S3D shows this model fitted to the experimental data, resulting in a good agreement. The length scaling of flowrate is therefore explained by the fact that an external circuit is necessary to measure the flowrate. This circuit has some fluidic impedance, which is more significant when the pumps are shorter. As the pumps become longer, the pump becomes a greater fraction of

the entire fluidic circuit and the impedance of the circuit matters less. Indeed, in the limit of an infinitely long pump, equation (11) tends to

$$Q_{lim} = \frac{Q_0 p_f}{p_f + Q_0 z_f} \qquad (13)$$

i.e. a constant value. This is the value of the asymptote marked on Fig. S3. This is also the flowrate that would be achieved if the measurement circuit were removed ($Z_s = 0$), by joining the pump ends together, for example. Note that this limiting value is not the same as the common flowrate value assumed at the beginning of this discussion (Q_0). This value of flowrate could only be achieved in the hypothetical scenario of a completely inviscid fluid ($z_f = 0, Z_S = 0$). This is an interesting result - even with no resistance to fluid motion, the flowrate is finite.

Supporting figures

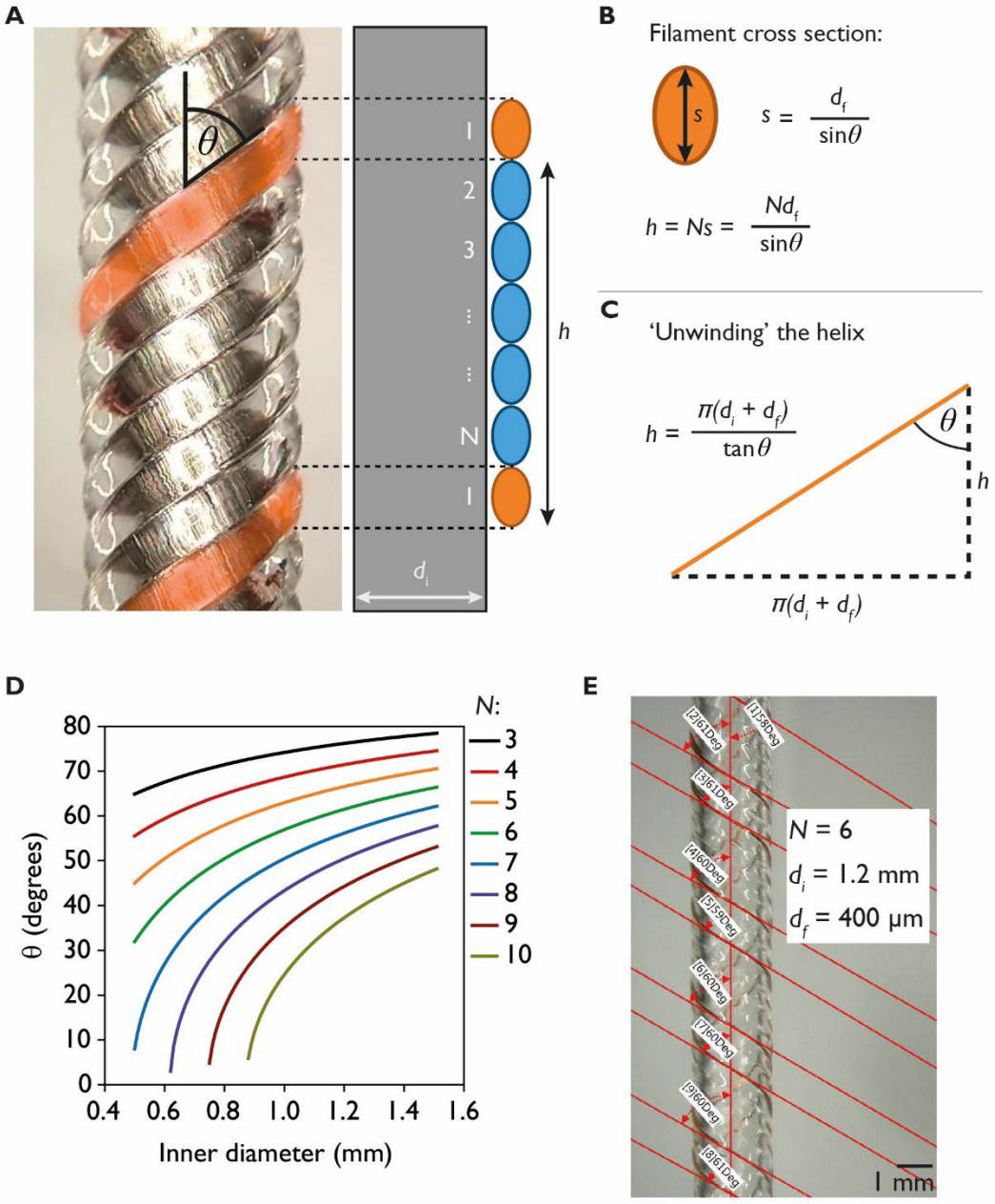

Fig S1. A model for filament winding. (**A**) A schematic representation of the cross section of *N* filaments fitting exactly within one helix pitch (*h*). (**B**) An expression for *h* in terms of the number of filaments, their diameter (d_f) and the helix angle θ. (**C**) Another expression for *h,* considering the path taken by the helix around the mandrel of diameter d_i. (**D**) The model prediction for helix angle as a function of inner diameter and number of filaments (*N*). Filament diameter is 400 µm in this plot. (**E**) Measurements of helix angle for a pump wound using 6 filaments, each 400 µm in diameter, around a 1.2 mm mandrel. The average angle is 60 ± 1 °, in good agreement with the model prediction.

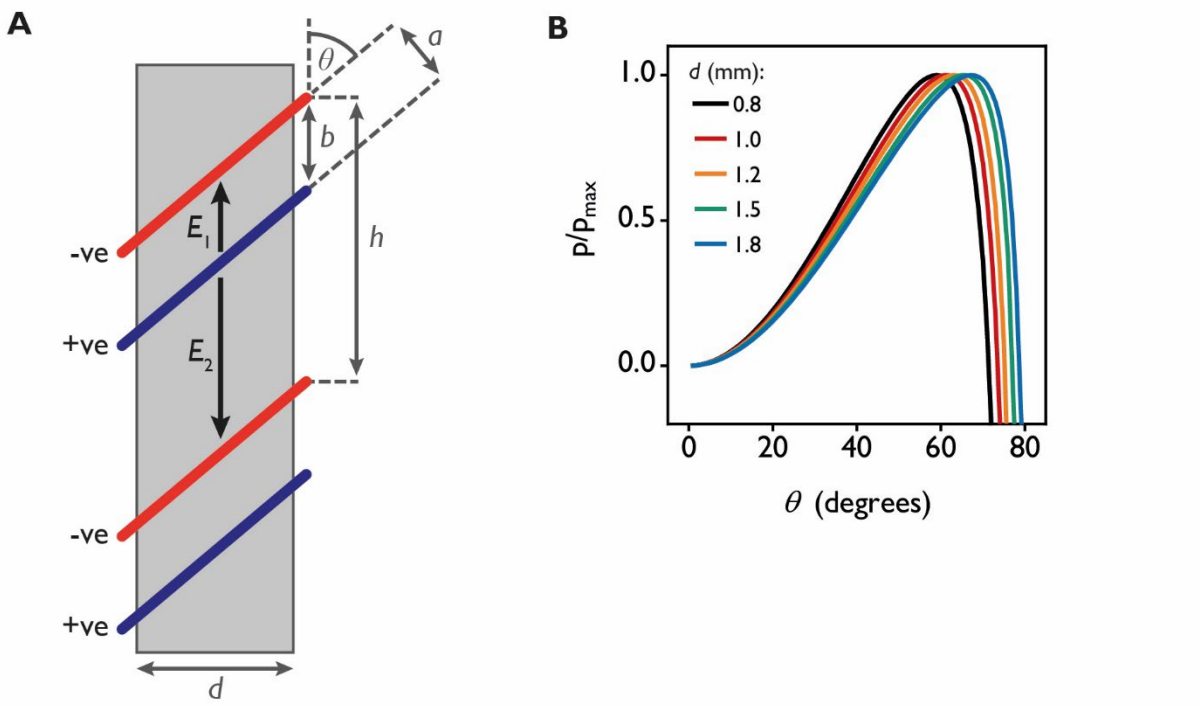

Fig S2. A first order approximation for the optimal helix angle. (**A**) The construction used during the approximation, with positive (+ve, blue) and negative (-ve, red) electrodes spaced perpendicularly by an amount *a***,** corresponding to a separation *b* when measured along the pump axis**.** The electrodes make an angle θ with the pump axis and have a pitch *h***.** The electric field parallel to the pump axis in the forward and negative directions are E_1 and E_2, respectively. (**B**) Plotting the pressure function (normalized to maximum value) for a range of internal diameters indicates the optimum helix angle for each condition. While each angle diameter has a different optimal angle, all angles are close to 60 °.

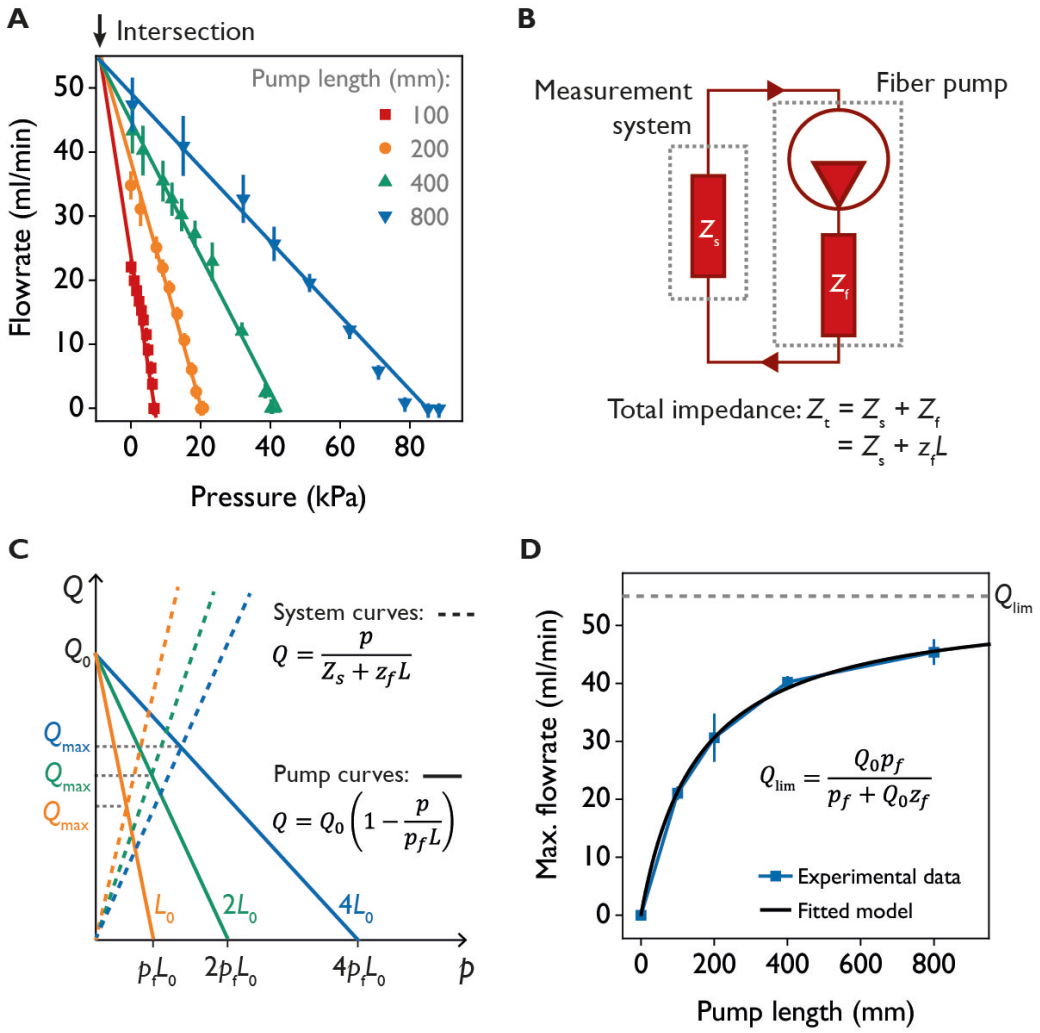

Fig S3. Rationalising the length scaling of maximum flowrate. (**A**) Experimentally observed pump curves for different lengths of fiber pump (aquired at 8 kV/mm). All four pump curves appear to intersect at a certain value of flowrate. (**B**) A model of the fluidic circuit used to chracterise the fiber pumps. The fiber pump is modelled by an ideal pump and an assocaited fluidic impedance Z_f. The impedance of the remainder of the circuit is Z_s. (**C**) A schematic of the fiber pump curves (solid lines) for 3 different lengths of pump: L_0, $2L_0$ and $4L_0$. The amount of pressure generated scales linearly with pump length at a rate of p_f. All curves intersect at the flowrate Q_0. Also drawn are the system curves for the 3 lengths of pump (dashed lines). The intersection of the pump curve and system curve gives the operating condition. (**D**) The hyperbolic model predicted by this analysis matches well with the experimentally observed length scaling of flowrate (data points are mean ± SD for $N = 3$ pumps).

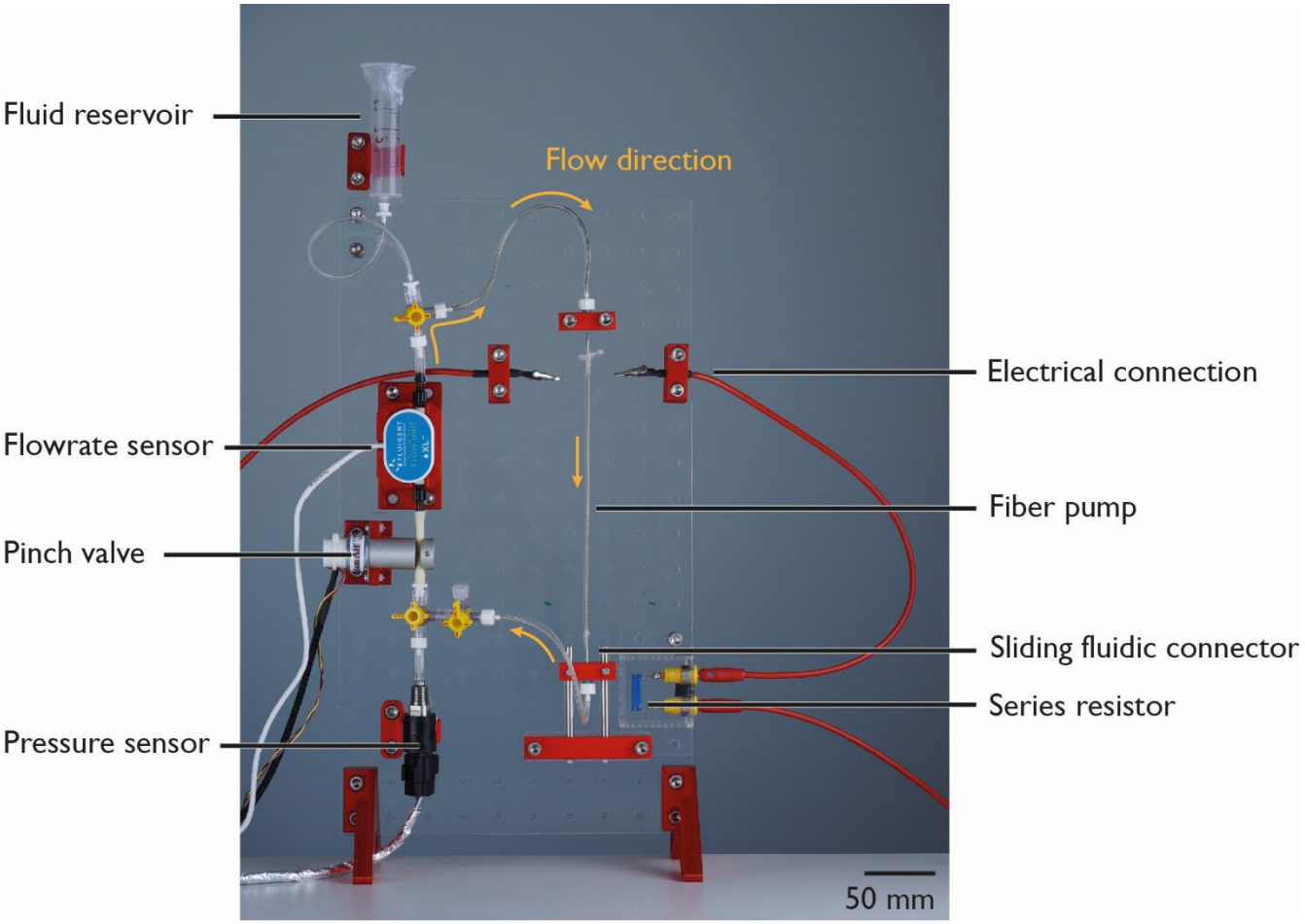

Fig. S4. The fluidic set-up used to characterize the fiber pumps.

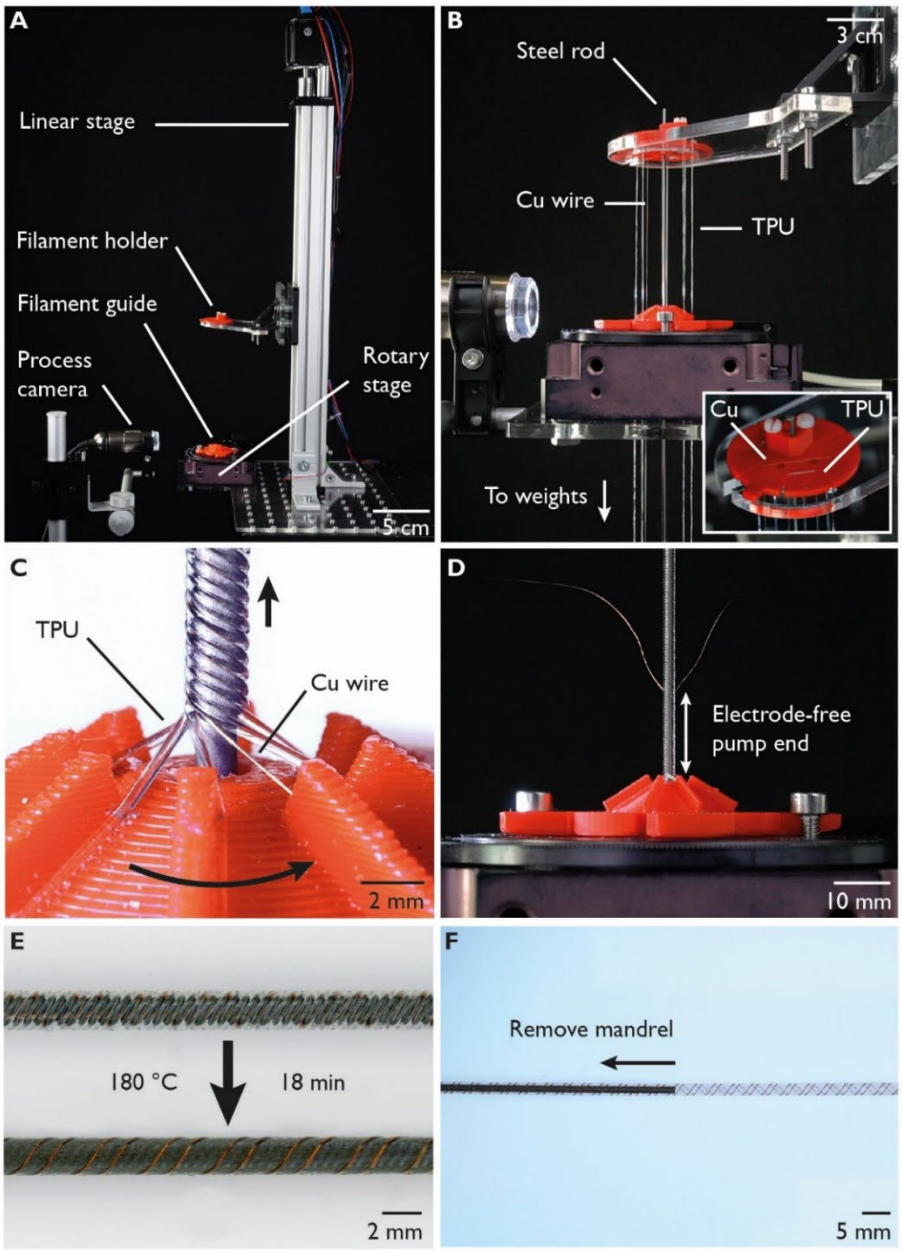

Fig. S5. The winding process used to fabricate fiber pumps. (**A**) The winding apparatus. (**B**) The apparatus with TPU filaments, Cu wire and central steel rod mounted. Of the 8 positions in the filament holder (inset), 6 are occupied by TPU and 2 with Cu wire. Two TPU filaments are mounted between the Cu wires to set the spacing of the helices. (**C**) During winding the Cu wire is taken in between and under the TPU filaments. (**D**) At the end of the pump, the Cu wire is pulled through the guide and winding continues to leave the end of the pump free from electrodes. (**E**) After winding, the structure is placed in an oven to melt and fuse together the TPU filaments. After fusing the Cu electrodes are visible. (**F**) Once fused, the mandrel can be removed. Prior to winding the mandrel is coated with a mold release spray to allow easy removal.

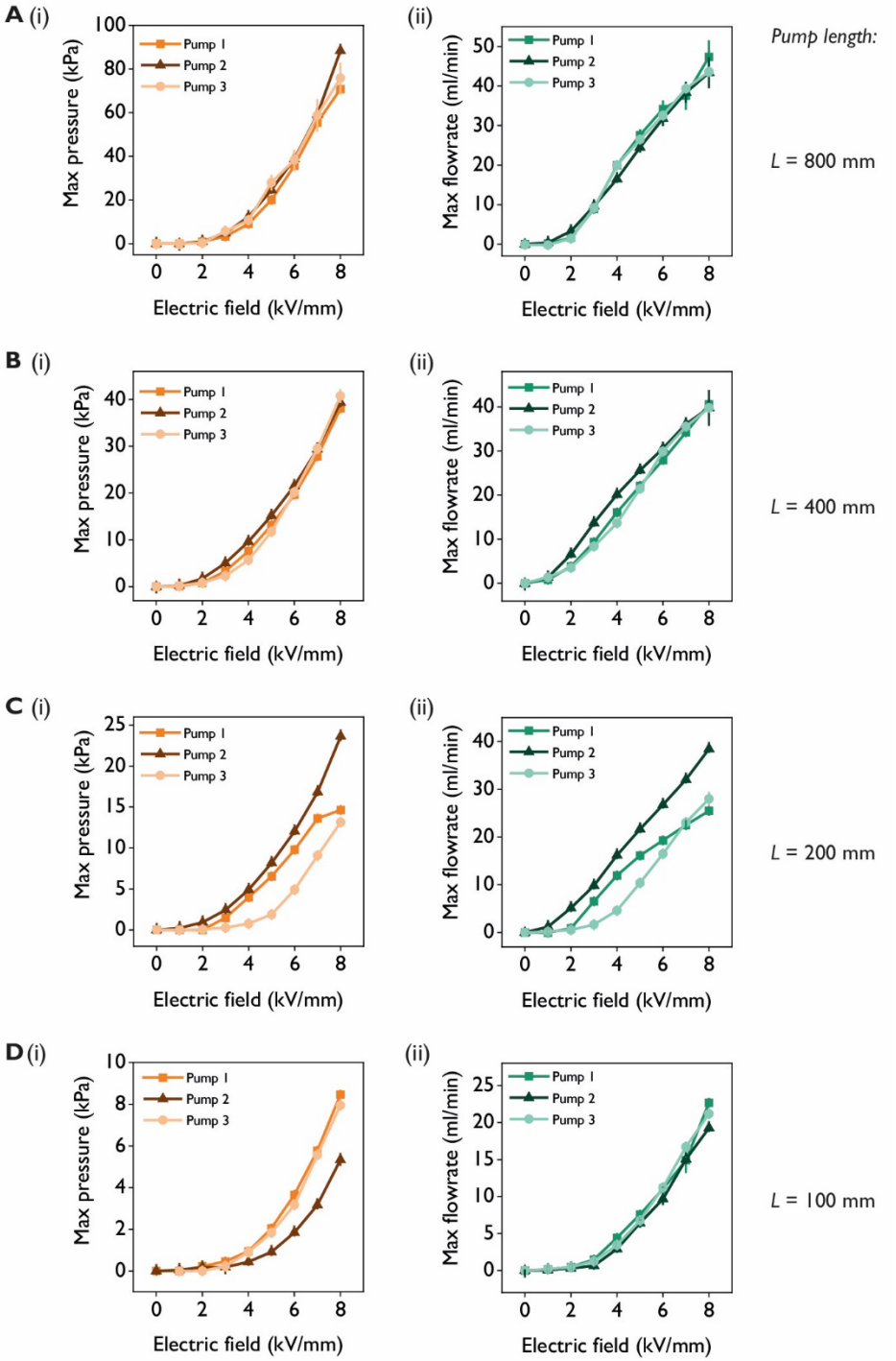

Fig. S6. Repeatability of fiber pump performance. The pressure and flowrate scaling of three pumps of each length: (**A**) 800 mm, (**B**) 400 mm, (**C**) 200 mm and (**D**) 100 mm. Each point corresponds to the average of 20 s of data at each electric field set point. Error bars are the standard deviation in the average value. The fiber pumps show excellent repeatability, which is often a problem for charge-injection EHD pumps.

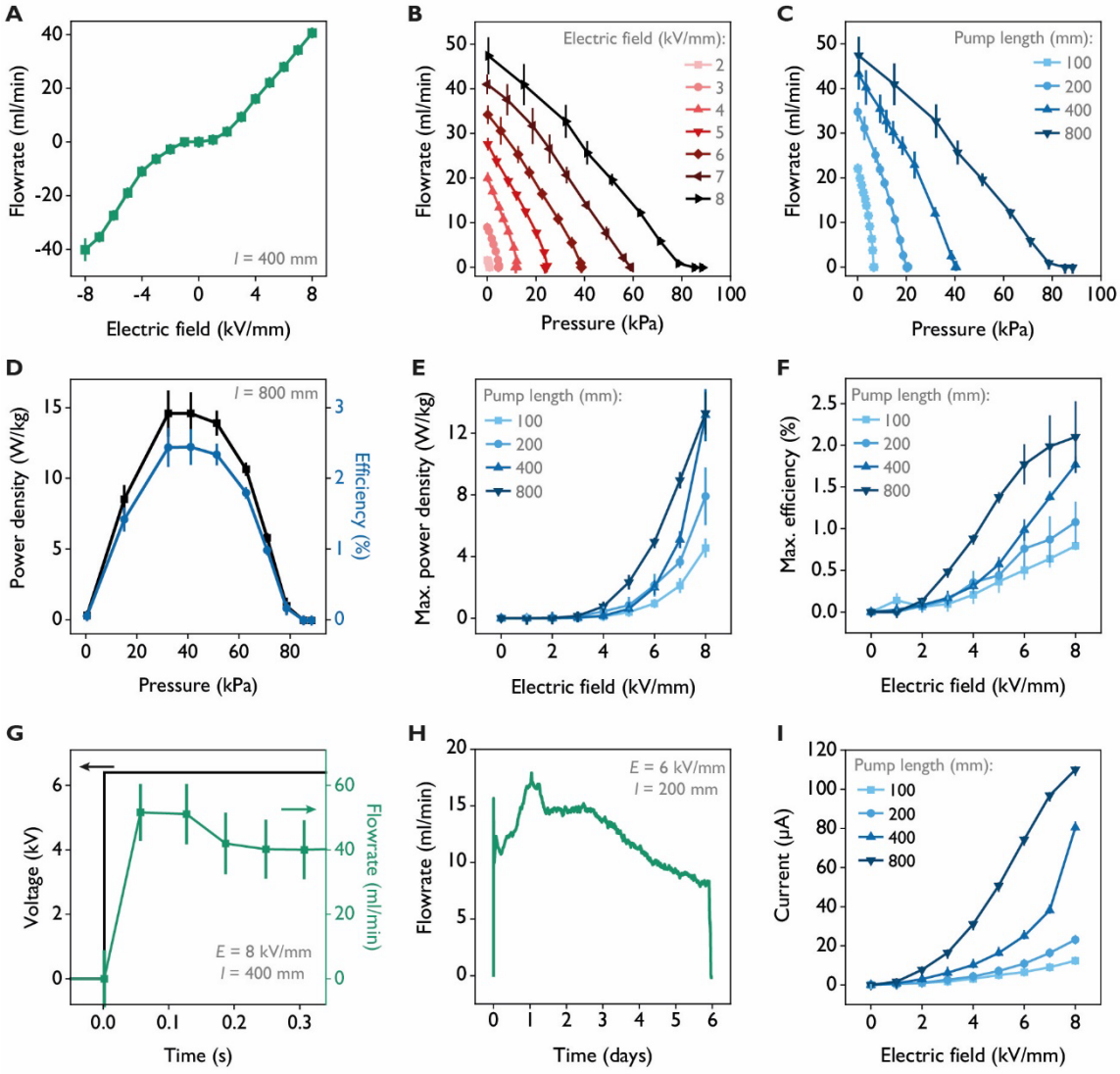

Figure S7. Additional pump data for fibers of 2 mm diameter (1.2 mm internal diameter). (**A**) Reversibility of flowrate. (**B**) The set of pump curves for an 800 mm pump in the electric field range [2-8] kV/mm. Data points represent the average of 10 seconds of data for a given position of the pinch valve. Error bars are the standard deviation in the average value. (**C**) The pump curves of fibers of different lengths, all acquired with an applied field of 8 kV/mm. (**D**) The power density and efficiency of one 800 mm fiber pump, operating at 8 kV/mm. Error bars are calculated from a propagation of uncertainty in the underlying pressure, flowrate, voltage and current measurements. Note that the linear pump curve results in maximum efficiency and power density at half the maximum pressure. (**E**) The maximum value of power density and (**F**) efficiency as a function of electric field, for $N = 3$ of each pump length. Error bars represent standard deviation in average value. (**G**) The response time of flowrate. The flowrate sensor used has a limited read rate of ~ 16 Hz. Error bars represent the error in the sensor calibration function. (**H**) Continuous operation of a 200 mm fiber pump at 6 kV/mm. Flowrate slowly decays due to passivation of the collecting electrode. (**I**) Current vs electric field for all the pump lengths tested.

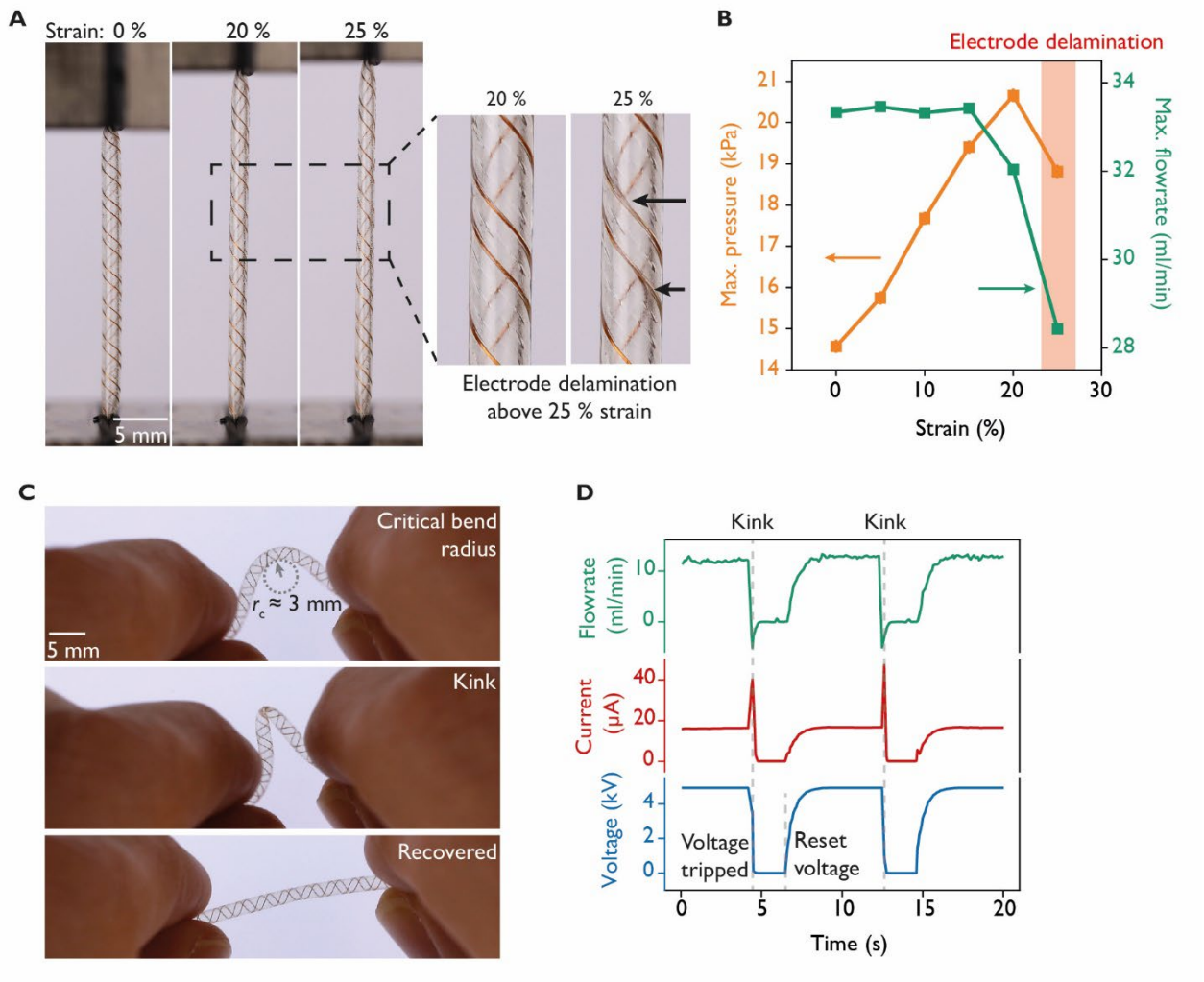

Figure S8. Mechanical limits of fiber pumps. All data is from pumps with 2 mm outer diameter. (**A**) Fiber pumps can withstand uniaxial strain up to 20 %. At 25 % strain the electrodes begin to delaminate, detaching from the polyurethane pump body. This is due to a mismatch in radial strain between the two components. In general, this detachment is not reversible. (**B**) Maximum pressure and maximum flowrate of a 200 mm long fiber pump subjected to uniaxial strain until failure. The pump continues to operate even as the electrodes begin to detach, albeit with reduced performance. Above 25 % strain, electrodes detach to the extent that short circuits are likely. (**C**) Kinking of the pumps occurs below a bend radius of ~ 3 mm, but the pump structure is not affected once the kink is removed. (**D**) Kinking will interrupt the pump output, often (but not always) causing an electrical breakdown in the liquid since the electrodes are brought closer together. The power supply is programmed to automatically turn off in the event of a breakdown. After releasing the kink and resetting the voltage, the flowrate returns to the original value.

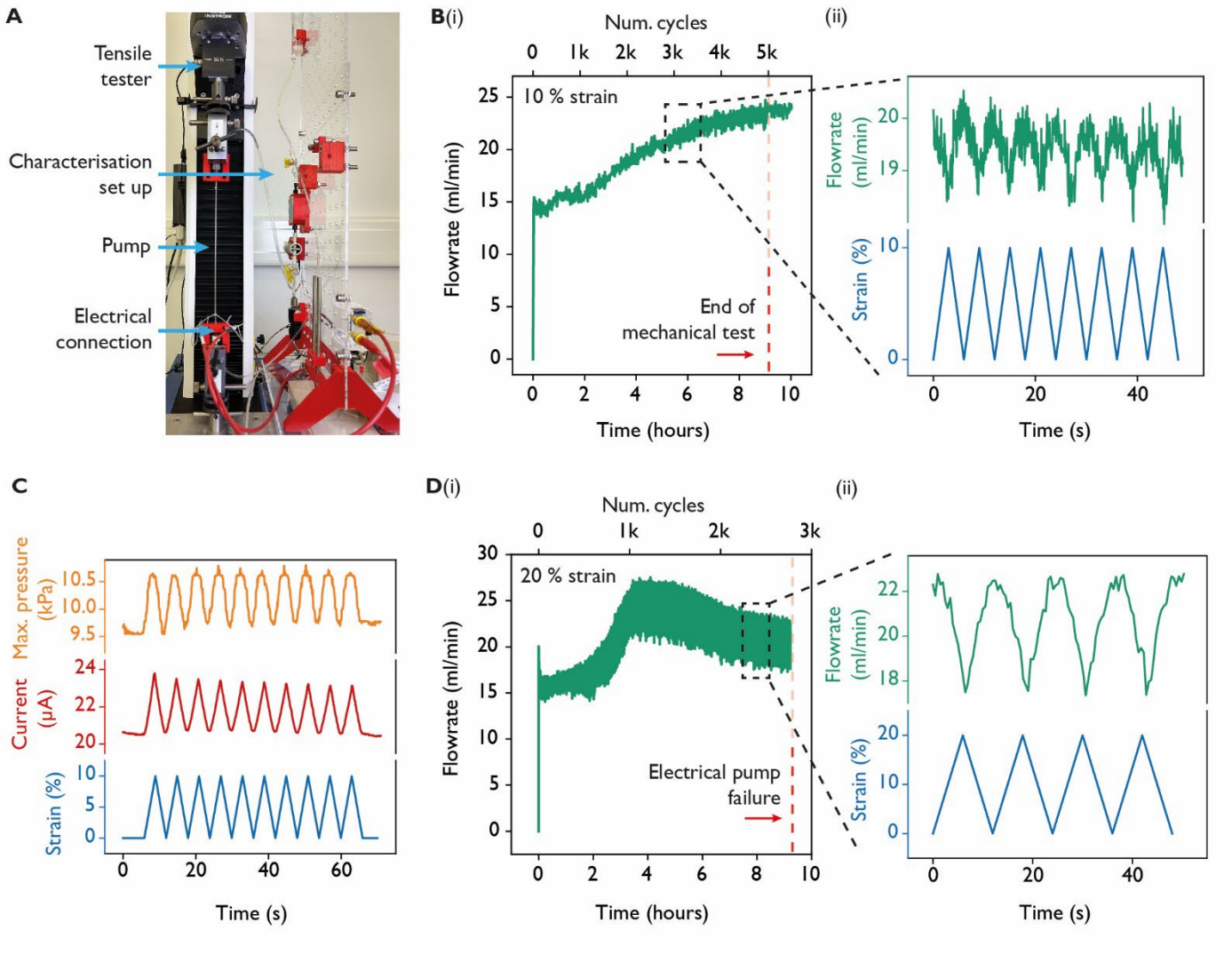

Figure S9. Dynamic strain response and fatigue. All data is from pumps with 2 mm outer diameter. (**A**) The pump and characterisation set up are installed in a tensile tester to determine the dynamic response to uniaxial strain and fatigue life. (**B**) Pump flowrate as a function of time while subjected to periodic deformation of 10 % uniaxial strain. The pump can withstand at least 5000 cycles (i) with no change to the performance. The increase of flowrate in time is also observed in undeformed pumps. The flowrate responds dynamically to the applied strain (ii), with flowrate decreasing as strain increases. (**C**) Pressure and current also respond to an applied strain, both maximized at maximum strain. (**D**) Pump flowrate as a function of time while subjected to periodic deformation to 20 % strain. (i) The pump fails due to an electrical short at approximately 2800 cycles. (ii) The dynamic response of flowrate to 20 % strain.

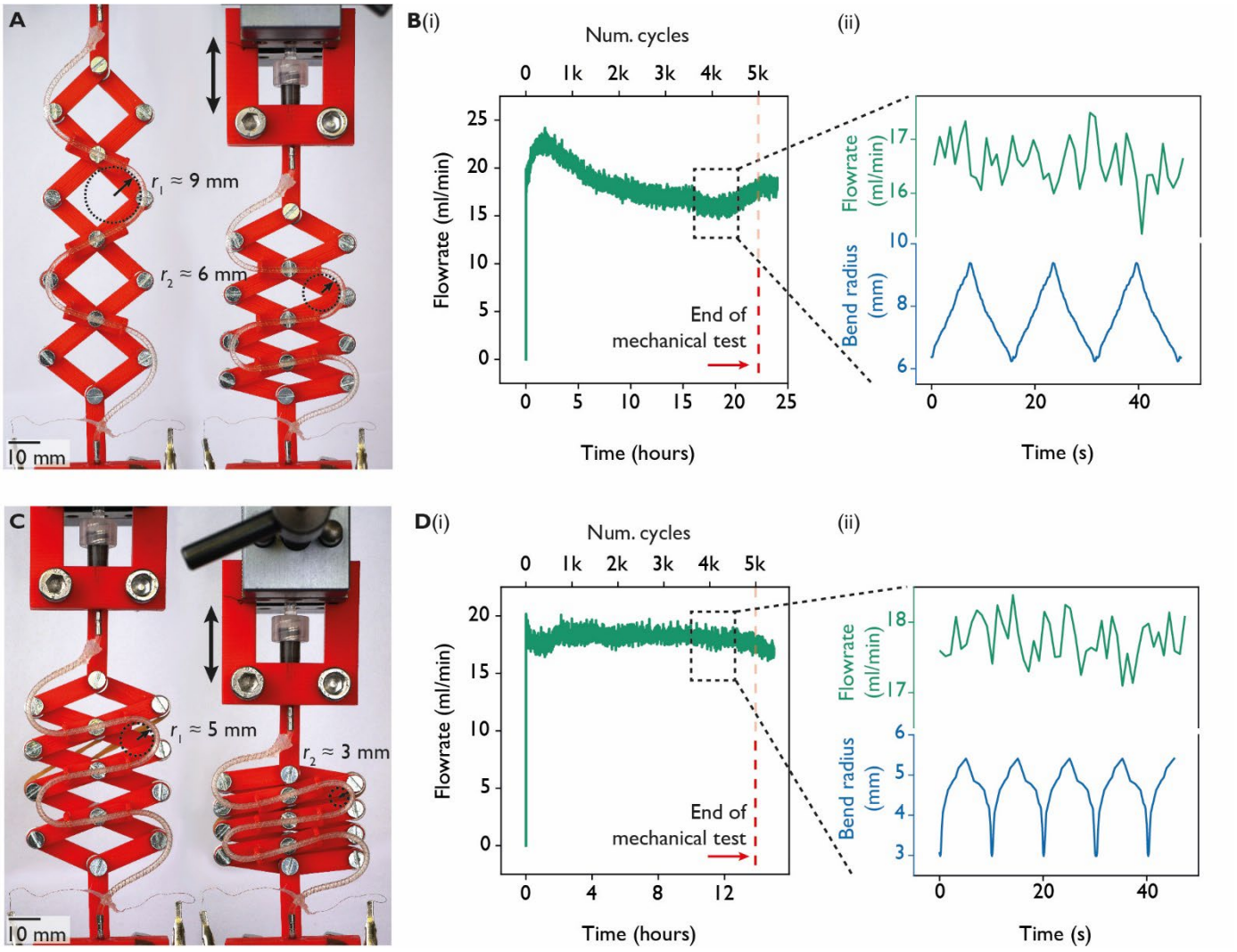

Figure S10. Dynamic flexion response and fatigue. All data is from pumps with 2 mm outer diameter. (**A**) A fiber pump mounted to a 3D printed scissor mechanism to repeatedly flex the pump between bend radii of 9 mm and 6 mm. (**B**) Flowrate as a function of time while the pump is subjected to repeated bending as shown in (A). The pump can withstand at least 5000 cycles (i) with no change in performance beyond what would normally be observed from an undeformed pump. (ii) Since only four points along the length of the pump are being deformed, there is no obvious correlation between flowrate and bend radius. (**C**) A second regime of pump flexion, varying the bend radius between 5 mm and 3 mm. (**D**) Flowrate as a function of time for a pump subject to the bending as shown in (C). The pump can withstand at least 5000 cycles (i) with no notable change in performance. (ii) Again, there is no obvious change in performance with bend angle.

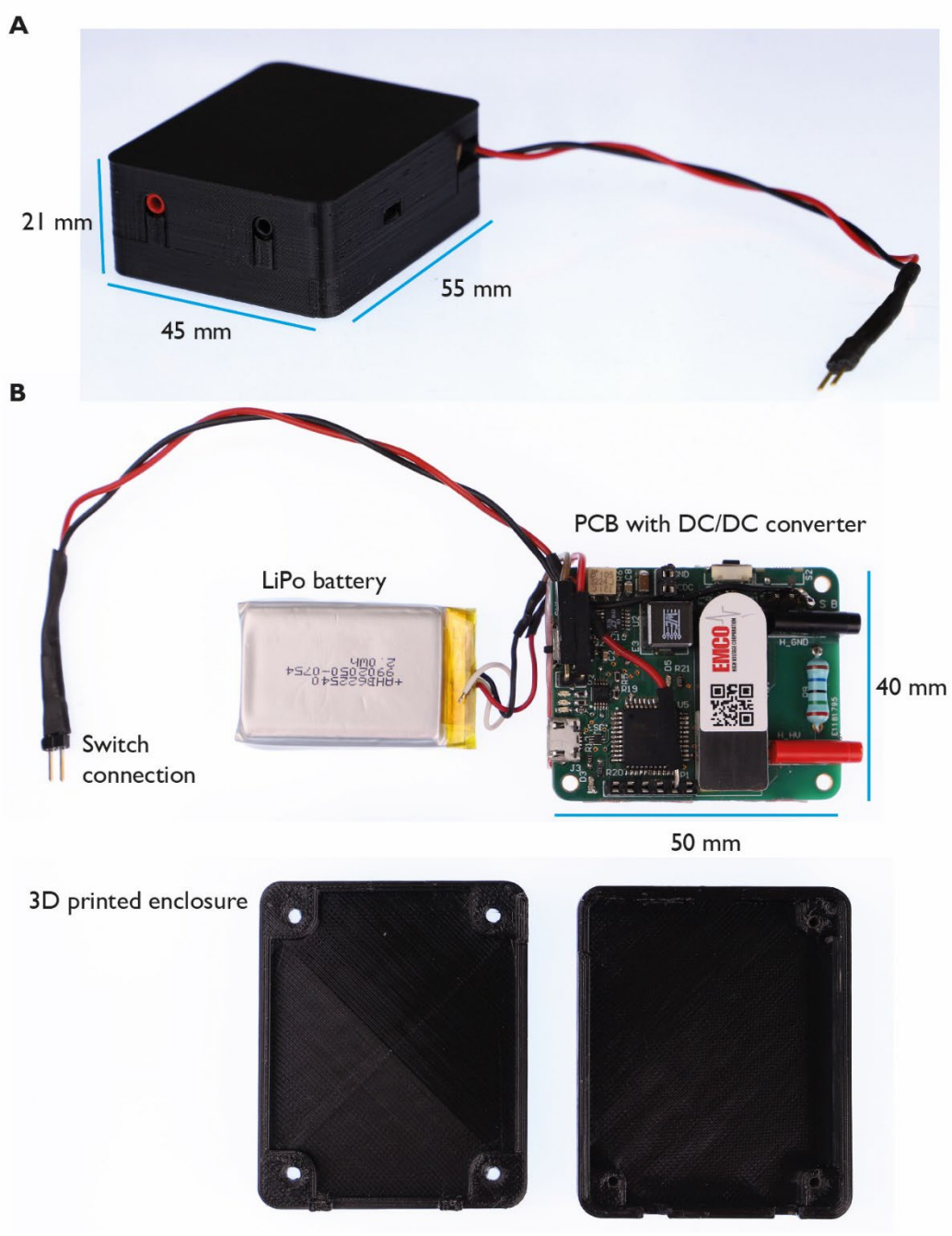

Figure S11. **A battery powered high voltage power supply**. (**A**) The power supply is compact and lightweight, weighing 35 g. (**B**) The PCB contains a 6 kV, 1.5 W EMCO DC/DC converter (AH60P – 5) which is powered by a 3.7 V, 550 mAh LiPo Battery (Renata ICP622540PMT). This particular battery can operate a 1-meter length of pump for approximately 2 hours. The high voltage output is activated via a switch, wired to the PCB with the connector shown.

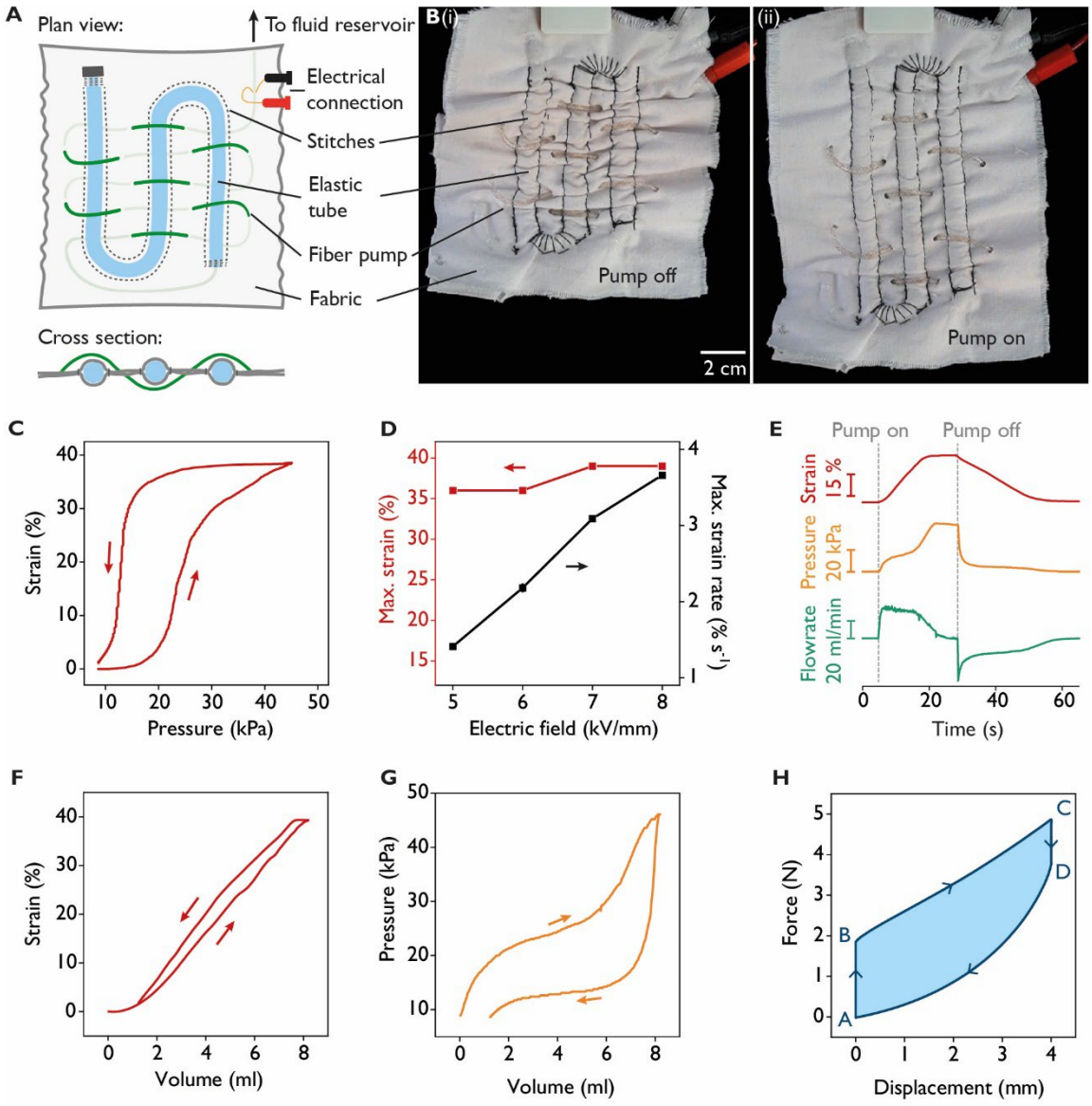

Fig. S12. Further characterisation of the fabric actuator. (**A**) A schematic of the fabric actuator with integrated fiber pump. (**B**) The actuator with (i) the pump off and (ii) the pump on, showing a 40 % strain with no weight attached. (**C**) The hysteretic response of strain as a function of pressure at a pump field of 8 kV/mm (**D**) The maximum strain and strain rate as a function of pump electric field. (**E**) The time response of the free-hanging actuator, operated at 8 kV/mm. (**F**) The strain-volume relationship for a pump field of 8 kV/mm. (**G**) The pressure-volume curve of the actuator at a pump field of 8 kV/mm. (**H**) A work cycle of the actuator, operating at 8 kV/mm. Loop begins at point A with the actuator fully pressurized. Pump is turned off to increase the axial force to point B, where the actuator is then strained to point C. Turning the pump on relaxes the axial force to point D, where the actuator is then contracted back to the original position A.

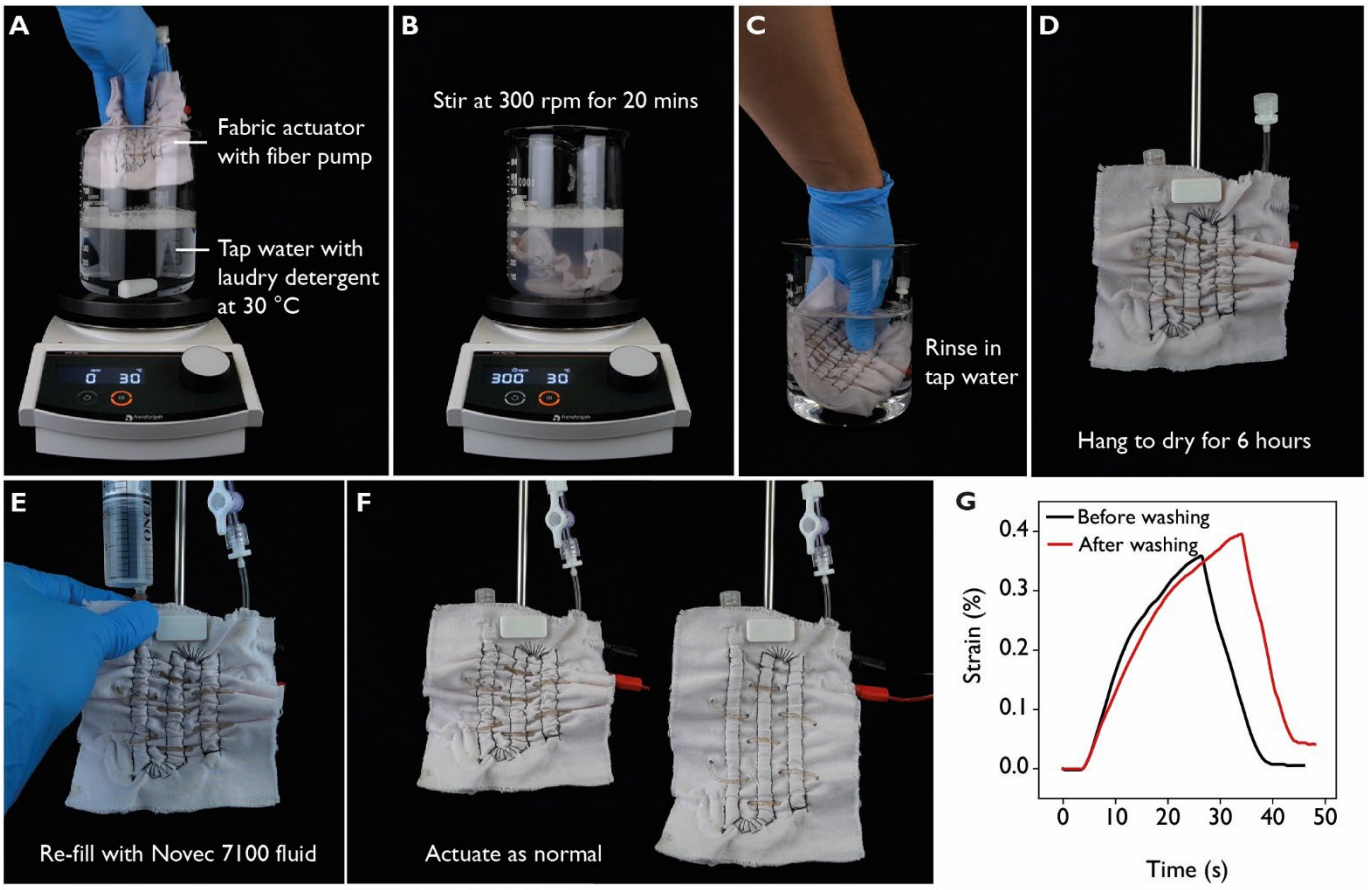

Fig S13. Demonstrating the washability of the fiber pumps. (**A**) The fabric actuator, as presented in figure 3 of the main text, is submerged in 30 °C tap water with standard laundry detergent. Prior to washing, the fluidic channels of the actuator are sealed. (**B**) Washing is simulated by stirring the liquid at 300 rpm for 20 minutes using a magnetic stirrer. (**C**) After 20 minutes the device is removed from the soapy water and rinsed in clean tap water several times. (**D**) The device is left to dry at room temperature in air for 6 hours. (**E**) Once dry the device is re-filled with fluid. (**F**) The device continues to operate as normal after this washing cycle. (**G**) The strain vs time of the device before and after washing. After washing and drying the structure of the device contracts a little, so for the first cycle after washing we obtain slightly more strain but do not return to the initial length.

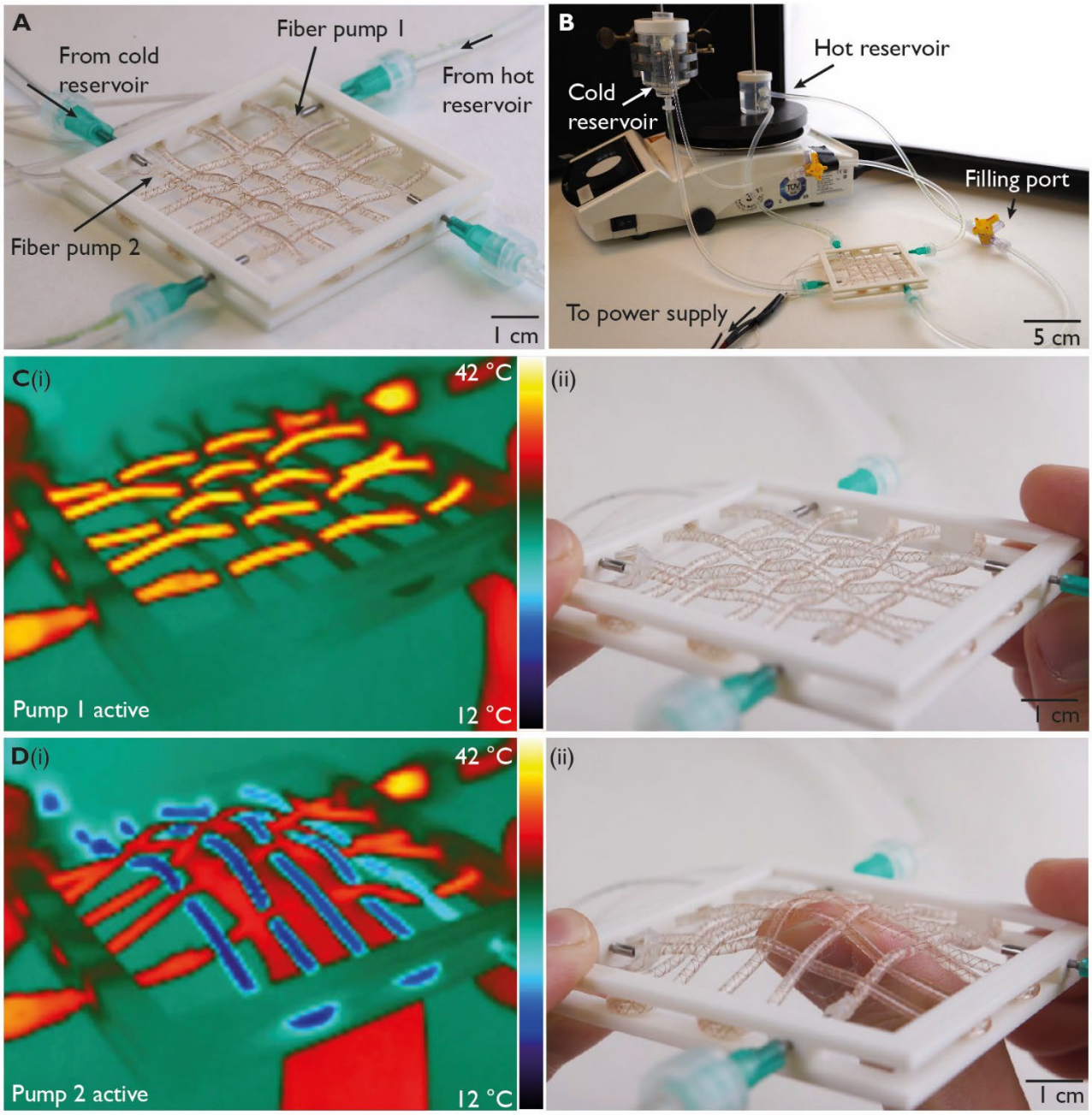

Fig. S14. Woven fiber pumps as a thermoregulatory fabric. (A) Two 400 mm fiber pumps, 2 mm in diameter, are woven together supported by a 3D printed frame. Pump 1 (the warp) is connected to a reservoir of hot fluid. Pump 2 (the weft) is connected to a reservoir of cold fluid. **(B)** The set up used to create this demonstration. A hotplate is used to heat the liquid, while water ice is used for cooling. Each pump and reservoir forms an independent, closed fluidic circuit. **(C)** A thermal image (i) and optical image (ii) of the woven pumps after pump 1 is activated, causing hot fluid to flow through the weave. **(D)** Thermal (i) and optical (ii) images was pump 2 is activated, cooling the woven pumps. Performance is maintained as the pumps are deformed (ii).

Mandrel diameter (mm)	Pump external diameter (mm)	Number of TPU filaments	Measured helix angle (degrees)
0.8	1.6	5	52
1.0	1.8	5	58
1.2	2.0	6	58
1.5	2.3	7	62
1.8	2.6	9	58

Table S1. Fabrication conditions for the pumps of different diameter but approximately constant helix angle. There is an error of ± 1 degree in the measured helix angle.

Pump outer diameter (mm)	Pump length (mm)	Max pressure (kPa)	Max flowrate (ml/min)	Mass (g)	Specific pressure (kPa/g)	Specific flowrate (ml/min/g)	Max power density (W/kg)	Power consumption (W)	Max efficiency (%)
1.6	200	24 ± 2	15.4 ± 0.5	0.23	106 ± 9	67 ± 2	6.9 ± 0.4	0.24 ± 0.01	0.73 ± 0.04
1.8	200	24 ± 1	32 ± 3	0.31	77 ± 5	103 ± 8	10 ± 2	0.23 ± 0.04	1.4 ± 0.2
2.0	200	21 ± 1	36 ± 1	0.34	62 ± 3	105 ± 3	11.0 ± 0.9	0.30 ± 0.04	1.36 ± 0.05
2.3	200	20 ± 1	52.0 ± 0.2	0.42	47 ± 10	123.8 ± 0.4	15.2 ± 1.0	0.37 ± 0.03	1.86 ± 0.02
2.6	200	12 ± 1	48 ± 2	0.54	22 ± 2	89 ± 3	6.2 ± 1.0	0.30 ± 0.03	1.16 ± 0.06
2.0	100	7.0 ± 1.5	21 ± 1	0.15	46 ± 10	140 ± 30	4.6 ± 0.5	0.09 ± 0.02	0.80 ± 0.02
2.0	200	21 ± 1	36 ± 1	0.34	62 ± 3	105 ± 3	11.0 ± 0.9	0.30 ± 0.04	1.36 ± 0.05
2.0	400	39 ± 1	40 ± 0.2	0.6	65.0 ± 1.7	66.7 ± 0.3	13.1 ± 1.6	0.48 ± 0.07	1.8 ± 0.1
2.0	800	80 ± 8	45 ± 2	1.2	67 ± 7	38 ± 2	13.3 ± 1.3	0.71 ± 0.02	2.1 ± 0.4

Table S2. Tabulated values of performance for the different geometries of fiber pump presented in this work. The values are mean values from measurements of three pumps of each type. Error is the standard deviation.

Pump	Ref.	Max pressure (kPa)	Max flowrate (ml/min)	Mass (g)	Specific pressure (kPa/g)	Specific flowrate (ml/min/g)	Max power density (W/kg)	Power consumption (W)	Max efficiency (%)
Fiber pumps:									
d1.6-l200	This work	24 ± 2	15.4 ± 0.5	0.23	106 ± 9	67 ± 2	6.9 ± 0.4	0.24 ± 0.01	0.73 ± 0.04
d2-l100	This work	7.0 ± 1.5	21 ± 1	0.15	46 ± 10	140 ± 30	4.6 ± 0.5	0.09 ± 0.02	0.80 ± 0.02
d2.3-l200	This work	20 ± 1	52.0 ± 0.2	0.42	47 ± 10	123.8 ± 0.4	15.2 ± 1.0	0.37 ± 0.03	1.86 ± 0.02
d2-l800	This work	80 ± 8	45 ± 2	1.2	67 ± 7	38 ± 2	13.3 ± 1.3	0.71 ± 0.02	2.1 ± 0.4
Soft pumps:									
Electrohydro-dynamic (EHD)	(*9*)	14	6	1	14	6	0.3[b]	0.17	0.2[d]
Electrohydro-dynamic (EHD)	(*12*)	9.2	423	3.0	3.1	141	5.2[b]	3.6	0.4[d]
Electro-pneumatic	(*11*)	2.34	161	5.3	0.5	30.5	0.3[b]	0.53	46.5[e]
Magnetohydro-dynamic	(*10*)	8	320	24[a]	0.3	13.5	0.9[c]	0.17	12.5
Combustion	(*13*)	60	40	54[a]	1.1	0.7	0.18[b]	-	-
Electromagnetic (rigid) pumps:									
Miniature solenoid pump	Gotec ESX-04	30	83.3	35	0.9	2.4	0.3[b]	5	0.2
Miniature gear pump	TCS MGD100S	1700	580	125	13.6	4.6	32[b]	52	7.6

Table S3. Comparing the performance of some selected fiber pump geometries with other reports of soft pumps and conventional miniature pumps. Selected fibers represent the maximum specific pressure, specific flowrate, power density and efficiency. The pump label refers to the diameter and length of pump: d2-l100 has outside diameter 2 mm and length 100 mm, etc.

[a] Mass not reported in reference. A lower bound of the mass has been calculated using the quoted device volume and densities of the materials used.

[b] Power density not reported in reference. An estimate has been calculated from the reported maximum flowrate (Q_{max}) and maximum pressure (p_{max}) using $\boldsymbol{P_d = \frac{1}{4} p_{max} Q_{max}}$. This estimate assumes a linear relationship between pressure and flowrate, as observed in the fiber pumps.

[c] Power density calculated from reported power consumption, efficiency and estimated mass.

[d] Efficiency not reported. An estimate has been made from the estimated power density and reported power consumption.

[e] Efficiency value reported in this reference is the peak instantaneous efficiency, occurring for approximately 100 ms. The operating efficiency is not reported.

Movie S1. Untethered operation of fiber pumps. A battery operated high-voltage power supply is used to operate a fiber pump, generating a jet of fluid. The voltage is turned on and off with a remote switch. The audio in the video highlights the silent operation of the fiber pump.

Movie S2. Manufacture of fiber pumps. A detailed description of the entire pump fabrication process, including the preparation of the raw materials, filament winding method and heat sealing.

Movie S3. Stretch- and flexibility of fiber pumps. A short demonstration of the flexibility and stretchability of the fiber pumps

Movie S4. Thermal haptic glove with fiber pumps. A demonstration of how fiber pumps can be used to create a thermal haptic glove. The video starts with an overview of the device, followed by activating each fiber pump separately in real time. An example use case is then presented, where pumps are activated as each finger comes into contact with an object, simulating the temperature of the object through thermal haptic stimuli.

Movie S5. Untethered thermoregulatory garment using fiber pumps. A demonstration of untethered fiber pump operation. Fiber pumps are attached to a t-shirt with a reservoir of chilled fluid and a battery-operated power supply. A hand-held switch activates the pumps, flowing chilled fluid around the garment.

Movie S6. Woven fiber pumps. Two fiber pumps are woven together to create a fluidic 'fabric'. One pump (the warp) is connected to a reservoir of hot fluid, while the second pump (the weft) is connected to a cold reservoir. Each pump is activated in turn, heating and cooling the fabric, which maintains its flexibility throughout.

Movie S7. Fluidic fabric muscle with integrated fiber pump. A fiber pump incorporated into a fabric actuator. The video begins with an overview of the device, then shows how the device is set up for demonstration. The video continues with a demonstration of free actuator extension/contraction, actuation with an applied load and operation in deformed states.

Movie S8. Inverse Hydraulic Artificial Muscle (IHAM) fibers. A demonstration of a fiber muscle, with both pump and actuator in fiber form. The video starts by highlighting the flexibility of the whole fiber, before showing the fast time response of a single fiber actuator. A bundle of three fibers then demonstrates the load bearing capacity, frequency response and repeatability.

Movie S9. Pump stability during deformation and kinking. A demonstration of how the fiber pump output (in this instance, flowrate) is broadly unchanged as the fiber pump is handled, bent and stretched. The pump is then kinked while in operation. This causes an electrical short circuit, which automatically turns the off the power supply. Releasing the kink shows the pump is undamaged and the flowrate returns to the previous level once the voltage is reset.

Movie S10. Washability of fiber pumps and fabric actuator. The fabric based artificial muscle is washed and dried to demonstrate washability of the pumps.